



IDENTIFICATION OF FIRST-IN-CLASS INHIBITORS OF KALLIKREIN-RELATED PEPTIDASE 6 THAT PROMOTE OLIGODENDROCYTE DIFFERENTIATION

Sabrina Aït Amiri, Cyrille Deboux, Feryel Soualmia, Nancy Chaaya, Maxime Louet, Eric Duplus, Sandrine Betuing, Brahim Nait Oumesmar, Nicolas Masurier, Chahrazade El Amri

► To cite this version:

Sabrina Aït Amiri, Cyrille Deboux, Feryel Soualmia, Nancy Chaaya, Maxime Louet, et al.. IDENTIFICATION OF FIRST-IN-CLASS INHIBITORS OF KALLIKREIN-RELATED PEPTIDASE 6 THAT PROMOTE OLIGODENDROCYTE DIFFERENTIATION. *Journal of Medicinal Chemistry*, 2021, 64 (9), pp. 5667-5688. 10.1021/acs.jmedchem.0c02175 . hal-03281511

HAL Id: hal-03281511

<https://hal.sorbonne-universite.fr/hal-03281511>

Submitted on 8 Jul 2021

HAL is a multi-disciplinary open access archive for the deposit and dissemination of scientific research documents, whether they are published or not. The documents may come from teaching and research institutions in France or abroad, or from public or private research centers.

L'archive ouverte pluridisciplinaire **HAL**, est destinée au dépôt et à la diffusion de documents scientifiques de niveau recherche, publiés ou non, émanant des établissements d'enseignement et de recherche français ou étrangers, des laboratoires publics ou privés.

1
2
3
4
5
6
7
8
9
10
11
12
13
14
15
16
17
18
19
20
21
22
23
24
25
26
27
28
29
30
31
32
33
34
35
36
37
38
39
40
41
42
43
44
45
46
47
48
49
50
51
52
53
54
55
56
57
58
59
60

IDENTIFICATION OF FIRST-IN-CLASS INHIBITORS OF KALLIKREIN-RELATED PEPTIDASE 6 THAT PROMOTE OLIGODENDROCYTE DIFFERENTIATION

Sabrina AÏT AMIRI¹ Cyrille DEBOUX², Feryel SOUALMIA¹, Nancy CHAAYA¹, Maxime LOUET³, Eric DUPLUS¹, Sandrine BETUING⁴, Brahim NAIT OUMESMAR^{2*}, Nicolas MASURIER^{3*}, Chahrazade EL AMRI^{1*}

- 1. Sorbonne Université, Faculty of Sciences and Engineering, IBPS, UMR 8256 CNRS-UPMC, ERL INSERM U1164, Biological Adaptation and Ageing, F-75252 Paris, France. Paris, France
- 2. Sorbonne Université, Inserm U 1127, CNRS UMR 7725, Institut du Cerveau, F-75013, Paris, France
- 3. Institut des Biomolécules Max Mousseron, Univ Montpellier, CNRS, ENSCM, Montpellier, France
- 4. Sorbonne Université, Faculty of Sciences and Engineering, IBPS, UMR 8246-CNRS / INSERM U1130 Neurosciences Paris Seine, F-75252 Paris, France. Paris, France

(*) Correspondence to C. El Amri (chahrazade.el_amri@sorbonne-universite.fr), B. Nait Oumesmar (brahim.nait_oumesmar@sorbonne-universite.fr); N. Masurier (nicolas.masurier@umontpellier.fr)

Abstract

Multiple sclerosis (MS) is an autoimmune demyelinating disease of the central nervous system (CNS) that causes severe motor, sensory and cognitive impairments. KLK6 is the most abundant serine protease secreted in the CNS, mainly by oligodendrocytes, the myelin-producing cells of the CNS, and KLK6 is assumed to be a robust biomarker of MS, since it is highly increased in the cerebrospinal fluid (CSF) of MS patients. Here, we report the design and biological evaluation of KLK6's low-molecular weight inhibitors, *para*-aminobenzyl derivatives. Interestingly, selected hit compounds were selective of KLK6 proteolytic network encompassing KLK1 and plasmin that also participate to the development of MS physiopathology. Moreover, hits were found non-cytotoxic on primary cultures of murine neurons and oligodendrocyte precursors (OPCs). Among them, two compounds (**32** and **42**) were shown to promote the differentiation of OPCs into mature oligodendrocytes *in vitro* constituting thus emerging leads for the development of regenerative therapies.

Keywords: Kallikrein-related peptidase 6; synthetic inhibitors; mechanism of inhibition; polypharmacology; demyelinating diseases; oligodendrocytes' maturation.

1
2
3
4
5
6
7
8
9
10
11
12
13
14
15
16
17
18
19
20
21
22
23
24
25
26
27
28
29
30
31
32
33
34
35
36
37
38
39
40
41
42
43
44
45
46
47
48
49
50
51
52
53
54
55
56
57
58
59
60

Introduction

Multiple sclerosis (MS) is a chronic inflammatory demyelinating disease of the central nervous system (CNS). MS affects more than two million people worldwide. ¹ In young adults, MS is the most common neurological disorder and the leading cause of severe non-traumatic disability. The main target of MS is the myelin sheath surrounding CNS axons in the brain, spinal cord and optic nerve. ¹ The myelin sheath is synthesized by oligodendrocytes that play a crucial role in the maintenance and functioning of neuronal networks. MS is associated with an inflammatory reaction of the CNS that results in degradation of the myelin sheath, therefore leading to diffuse demyelinating lesions. The consequences of this demyelination are multiple, nerve conduction is impaired and neurodegeneration occurs with disease progression. ² Moreover, myelin debris exacerbates the activation of immune pathways triggering demyelination. ³ Clinically, these disturbances result in severe motor, sensory and cognitive deficits. The lack of a regenerative therapy that prevents disease progression represents the greatest unmet medical in MS. Disease-modifying drugs in the market are mainly targeting the inflammatory components of the pathology, but have little impact on oligodendrocyte regeneration and remyelination. ⁴⁻⁶ The identification of new therapeutic compounds for MS-enhancing myelin repair is thus a critical public health issue. ^{7, 8} A special effort may be put on the search for pharmacological compounds, capable of simultaneously modulating neuroinflammation and promoting myelin regeneration for a more complete health care of MS patients. There is thus an urgent need to identify and validate novel targets to reach this issue.

In adults, under normal physiological conditions, kallikrein-related peptidase 6 (KLK6) is strongly expressed by oligodendrocytes and can be detected in neurons, whereas it is very weakly expressed in astrocytes and resting microglia. ⁹ However, in response to a CNS lesion

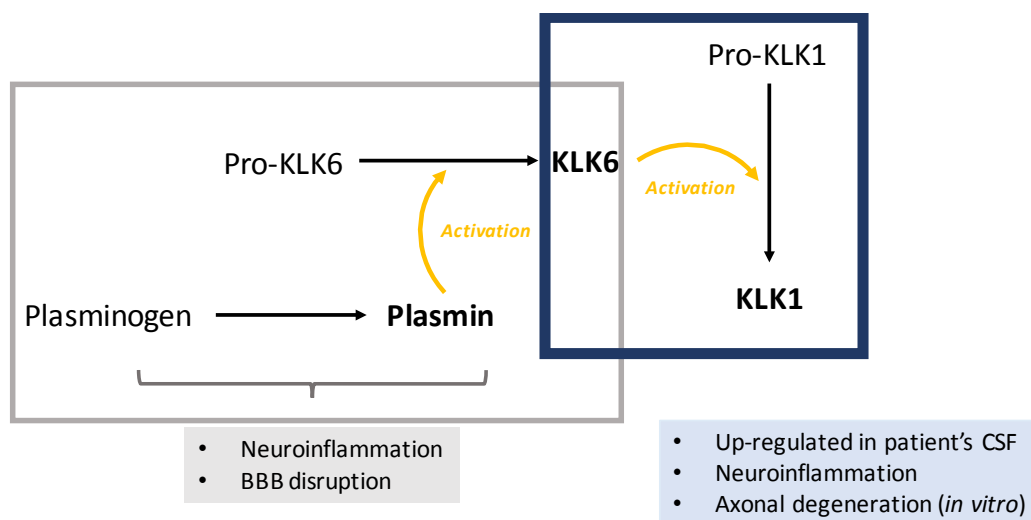
1
2
3 such as glutamate-induced excitotoxicity, inflammation or traumatic injury, the level of KLK6
4
5 expression rises in oligodendrocytes and neurons, and its expression is induced in reactive
6
7 astrocytes and microglia. ¹⁰ Among the 15 tissue kallikreins, KLK6 is the most abundant in the
8
9 CNS, and is arguably the most abundant serine proteases produced in the CNS. ¹¹
10
11

12
13 KLK6 has a versatile action within the CNS. ⁹ Interestingly, KLK6 cleaves myelin proteins,
14
15 such as the myelin basic protein (MBP). KLK6 is a major protease of the process of
16
17 demyelination/remyelination of axons. ^{9, 10, 12} In addition to cleaving myelin proteins, KLK6 can
18
19 also degrade blood-brain barrier components such as laminin, fibronectin and collagen, and
20
21 induces inflammation *via* Protease Activated Receptors (PAR) activation and underlying
22
23 intracellular Ca²⁺ mobilization. It should also be noted that the use of recombinant KLK6 *in*
24
25 *vitro* contributes to neuronal lesions and oligodendroglipathies. ¹³ Some proteases have also
26
27 been suggested for the activation of KLK6 *in vivo*, including plasmin, a serine protease involved
28
29 in fibrinolysis. Finally, KLK6 is involved in oligodendrocyte differentiation and myelination
30
31 processes. Different studies support that KLK6 is involved in the pathophysiology of MS. ¹²⁻¹⁷
32
33 Firstly, patients with MS have abnormally high KLK6 levels in serum, cerebrospinal fluid (CSF)
34
35 and demyelinating lesions, which demonstrate the implication of this protease at different
36
37 levels of the pathology. ¹⁸ Secondly, KLK6 induces demyelination, both through excessive
38
39 cleavage of myelin proteins and deleterious effects on oligodendrocyte-process outgrowth
40
41 and differentiation, thus leading to a drastic reduction in the number of myelinating
42
43 oligodendrocytes. ¹⁹ Third, KLK6 participates in the neuroinflammatory process through the
44
45 overactivation of PAR receptors but also by increasing the expression of pro-inflammatory
46
47 cytokines. Therefore, KLK6 participates in the establishment of a toxic environment that leads
48
49 to demyelination and neurodegeneration, the main cause of disability progression in MS
50
51 patients. ¹⁹ KLK6 and KLK1 may also serve as serological markers of MS and may contribute
52
53
54
55
56
57
58
59
60

1
2
3
4
5
6
7
8
9
10
11
12
13
14
15
16
17
18
19
20
21
22
23
24
25
26
27
28
29
30
31
32
33
34
35
36
37
38
39
40
41
42
43
44
45
46
47
48
49
50
51
52
53
54
55
56
57
58
59
60

directly to neurodegeneration. Furthermore, the immunization of mice with recombinant KLK6 antibodies significantly delayed onset and severity of clinical deficits in an experimental autoimmune encephalomyelitis (EAE) mouse model of MS.^{12, 20} It is also well established that the potential significance of proteolytic activity in MS not only relates to their use as potential biomarkers but also as prospective therapeutic targets. The range of potential involvement of proteolytic activity in MS pathogenesis extends from parenchymal degenerative events including myelin destruction and axon injury, to release of antigenic self-epitopes, immune cell activation, and permeabilization of the blood-brain barrier. Scarisbrick and co-workers have proposed the term of MS degradome to encompass the set of proteases, substrates, and endogenous protease inhibitors involved in development and progression of MS.¹⁹

Scheme 1 summarizes the central role of KLK6 and its crosstalk with thrombolytic proteolytic pathways, thus illustrating the early concept of MS degradome.²¹ Particularly, it has been recently shown that plasminogen and plasmin-mediated fibrinolysis are key modifiers of the onset of neuroinflammatory demyelination.^{22, 23} KLK1 was early shown to be a potential serological marker of progressive MS and contribute directly to the development of neurological disability by promoting axonal injury and neuron apoptosis.¹⁹



Scheme 1: Putative KLK6's pathological proteolytic network

In this context, the development of innovative inhibitors of KLK6 activity and its associated proteolytic network appears as a new therapeutic avenue.

The aim of this study is thus to identify potent KLK6 inhibitors encompassing the following properties: (i) reversibility, indeed non-covalent inhibitors, which are devoid of a reactive group, do not have the drawbacks generally associated with the presence of a warhead, such as lack of specificity, instability and excessive reactivity. Considering the physiological implication of KLK6 in the CNS homeostasis reversible inhibition would be safer, and (ii) able to inhibit other proteases involved in the KLK6 proteolysis network, *i.e.* KLK1 and plasmin. Herein, we identified and optimized original organic inhibitors for KLK6 and its proteolytic network. The designed low molecular weight inhibitors are potent and reversible towards KLK6, their inhibitory potency was also evaluated on a large panel of proteases. We also provided a detailed structure-activity relationship and dissected out the chemical basis for optimal inhibition. Hit compounds were found devoid of cytotoxic effects towards

primary cultures of mouse neurons and oligodendrocyte precursors (OPCs), and displayed favorable drug-like characteristics. Interestingly, some hit compounds promoted OPC differentiation *in vitro*. These selected compounds constitute promising leads for the development of innovative myelination therapy.

Results and Discussion

Rational design of para-benzylamine derivatives

While the field of KLK’s inhibitor discovery is relatively underdeveloped despite very huge interest in several therapeutic areas, recent reviews highlight the interest and need for further works.²⁴⁻²⁸

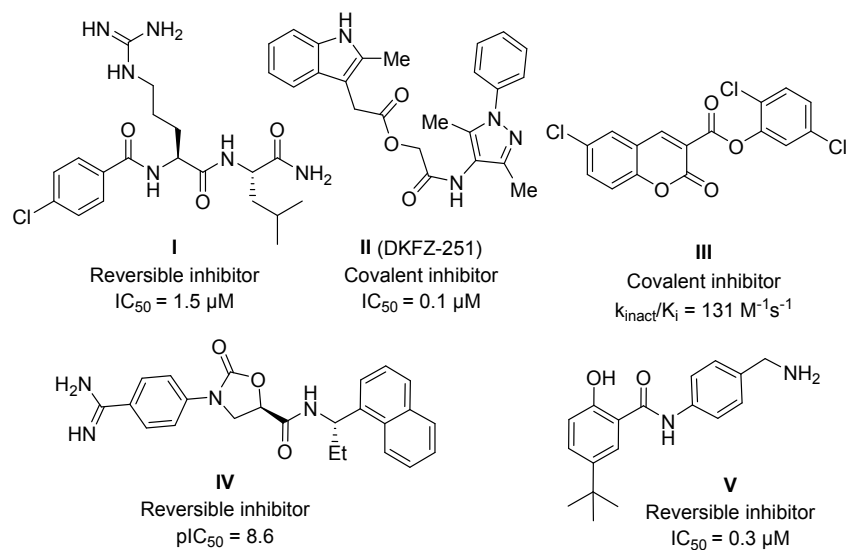


Chart 1: Main KLK6 inhibitors reported in the literature

A common approach for the development of inhibitors has been to use natural peptide inhibitors as starting points, exploiting combinatorial or designed mutations in order to achieve selectivity toward the targeted KLK (*e.g.* compound I, Chart 1).^{24, 28} However, the development of subtype selective KLK inhibitors remains challenging. Papo and collaborators

developed a yeast-displayed mutant library of the human amyloid precursor protein Kunitz protease inhibitor domain (APPI) to derive serine protease inhibitors especially of KLK6.²⁹ Recently, Miller and co-workers have reported depsipeptides as potent KLK6's inhibitors to derive activity-based probes (Compound II, Chart 1).³⁰ Our team has also recently identified 6-substituted coumarin-3-carboxylate derivatives as mechanism-based inhibitors (suicide substrates, compound III, Chart 1).³¹ Several small molecules were also reported as reversible inhibitors of KLK6. Among them, benzamidine and benzylamine derivatives are probably the most potent inhibitors (*e.g.* compounds IV and V, Chart 1).^{32,33} Especially, *N*-(4-aminomethyl-phenyl)-2-hydroxy-benzamide derivatives reported by Liang and co-workers are easily accessible and can be subjected to a large chemical diversification for structure-activity relationship (SAR) studies. Moreover, these compounds can potentially provide access to submicromolar inhibitors. In this study, nine analogs were described and the 5-*tert*-butyl derivative (compound V, Chart 1) revealed to be the most potent inhibitor of this series (IC_{50} = 0.3 μ M) constituting an initial hit.³³ Substitution of the methylene group of the benzylamine as well as alkylation at the amino nitrogen led to inactive compounds, which clearly demonstrates that the amino group of the benzylamine is mandatory for the KLK6 inhibition. X-ray structure obtained with one of the derivatives of this series revealed that the benzylamine group bound into the S1 pocket of KLK6 by sharing a primary amine H-bonding with the side chain of N189. The side chain of I218 is also an important factor to the binding affinity through hydrophobic interaction with the phenyl ring of the benzylamine moiety. The hydroxyl group of the phenol occupied the center of the oxyanion hole, forming an H-bonding network with the backbone NH groups of G193 and S195 (**Figures 1A and B**). Keeping constant these key elements involved in KLK6 interaction (**Figure 1C**), we synthesized and evaluated novel series of *N*-(4-aminomethyl-phenyl)-2-hydroxy-benzamide and hydroxynaphtamide

derivatives and identified drug-like reversible organic inhibitors of KLK6 and its associated proteolytic network.

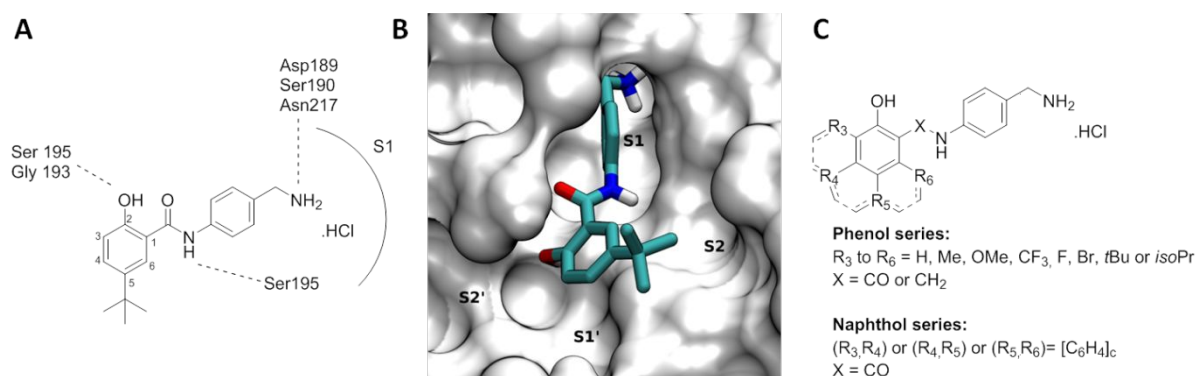
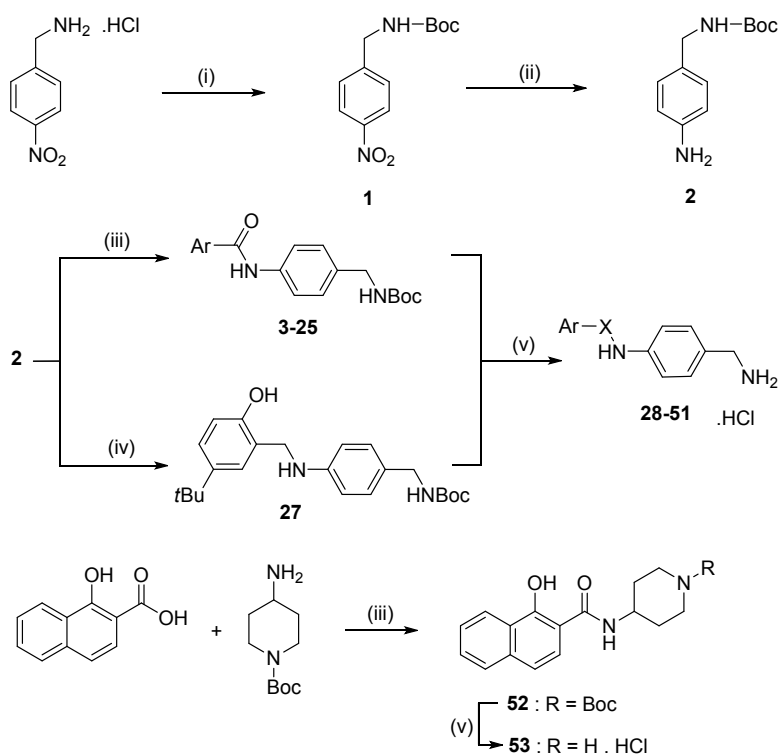


Figure 1: Rational design of *para*-amidobenzyl derivatives. **A.** Key interactions of compound **V** in the active site of KLK6 (H bonds are shown as dashed lines); **B.** Positioning of compound **V** in the S1 and S1' pockets of KLK6; **C.** Structures of studied compounds.

Targeted compounds, as well as the reference compound **V** (now named compound **28**) were synthesized as reported in Scheme 2.

Briefly, compound **2** was obtained in two steps from 4-nitrobenzylamine hydrochloride after Boc protection of the amine group, followed by the reduction of the nitro function. Compound **2** was then coupled with the appropriate salicylic or naphthoic acid in presence of EDCI (*N*-(3-dimethylaminopropyl)-*N*'-ethylcarbodiimide hydrochloride) to offer compounds **3-25** in moderate yields. Compound **27** was synthesized by reductive amination with aldehyde **26** in presence of sodium borohydride. Reaction between 1-naphthoic acid, 1-Boc-4-aminopiperidine and EDCI offered compound **52** in 64% yields. Finally, Boc group was removed using a mixture of hydrochloric acid in 1,4-dioxane to offer compounds **28-51** and **53** as hydrochloride salts.



Reagents and conditions: (i) Boc_2O , TEA, DCM, RT, 2h, 80%; (ii) H_2 , 10% Pd/C, AcOEt, RT, 4h, qt; (iii) ArCO_2H , EDCI, THF, reflux, 12h, 12-82%; (iv) 1. Compound **26**, EtOH, reflux, 6h; 2. NaBH_4 , RT, 1.5 h, 64% and (v) 6N HCl gaz in 1,4-dioxane, RT, 1.5 h, 44-99%.

Scheme 2: Synthesis of compounds **1** to **53**

Inhibitory potency hit compounds on KLK6 and on its proteolytic network

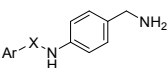
Newly synthesized compounds **28-51** and **53** were first screened on KLK6 through the evaluation of the percentage inhibition at 10 μM . This allows highlighting the promising compounds for the inhibition of KLK6. Among the 25 designed compounds, we preselected those raising an inhibition of at least 50% of the activity of KLK6 at a concentration of 10 μM and then determined their inhibitory potency through the quantification of IC_{50} .

Starting from reference compound **28** (Table 1) previously identified by Liang and al. (2012a), several modifications were studied in the phenol series, in order to determine key structural elements for KLK6 inhibition. Suppression of the carbonyl group (compound **29**) as well as the *tert*-butyl group (compound **30**) led to the loss of the activity. Then, sensitivity to the position of the substituent carried out by the phenol group was observed in the methyl series (compounds **31** to **34**). Substitution of position 4 and position 5, in a less extent, were the most favorable to observe an optimal inhibition of KLK6. Several other groups were then introduced into C4 and C5. These positions must be substituted by an apolar or bulky group such as an isopropyl (compound **37**) or a methyl group (compound **32**) for C4 substituted derivatives and a *tert*-butyl group (compound **28**) for C5 substituted derivatives. Interestingly, the substitution of the C5 position by a halogen (compound **35**) or by a methoxy group (compound **36**) is strongly unfavorable for the inhibition of KLK6.

When the inhibitor contains a naphthol group, a slight sensitivity with respect to the position of the hydroxyl group is observed. Indeed, it must be substituted at positions 1 or 3 for optimal inhibition of KLK6 (compounds **40** and **42** respectively). More generally, the hydroxyl group is essential because the inhibition of KLK6 decreases drastically when the inhibitor contains a naphthyl (compound **43**) instead of a naphthol. This result is not surprising because, in the phenol series, the hydroxyl group was reported to be involved into key interactions notably with the S195 residue of KLK6. There is also a lack of inhibitory effect when the compound contains an indolyl (compound **44**) or an oxoquinolyl ring (compound **45**) in place of the naphthol ring, indicating that the hydroxyl group could not be replaced by another hydrogen donor or acceptor (NH or ketone). Moreover, we noted the importance of the benzylamine group. Indeed, we observed a significant decrease in the inhibition when this same position is occupied by a piperidinyl group (compound **53**). Finally, several substitutions

into the naphthol ring were studied (compounds **47** to **51**, see supplementary information). However, all studied modifications led to autofluorescent compounds that could not be evaluated, except when a methoxy group was introduced on position 6 (compound **47**). In this case, a slight loss of activity compared to its unsubstituted analog (compound **40**) was observed.

Thus, among the new synthesized compounds, 5 new hits were identified in the series of *para*-aminobenzyl compounds (molecules **32**, **37**, **40**, **42** and **47**) (Table 1), displaying IC₅₀ equal or below 5 μM. The IC₅₀ accounts for the effectiveness of the inhibitor with respect to the enzyme and allows a prioritization according to the inhibitory power. The IC₅₀ values place compounds **32** and **42** at the top, while reference compound **28** (IC₅₀ = 9.06 μM) has one of the lowest efficacy with respect to KLK6 among the selected inhibitors.

Compound	Ar	X	% Inhibition at 10 μM or IC ₅₀ (μM)
			
28	5- <i>tert</i> -butyl-2-hydroxyphenyl	CO	9.06 ± 0.65
29	5- <i>tert</i> -butyl-2-hydroxyphenyl	CH ₂	NI
30	2-hydroxyphenyl	CO	14.83 %
31	3-methyl-2-hydroxyphenyl	CO	20%
32	4-methyl-2-hydroxyphenyl	CO	2.37 ± 0.12
33	5-methyl-2-hydroxyphenyl	CO	26.47 %
34	6-methyl-2-hydroxyphenyl	CO	7.27 %
35	5-bromo-2-hydroxyphenyl	CO	29.98 %
36	5-methoxy-2-hydroxyphenyl	CO	21.83 %
37	4-isopropyl-2-hydroxyphenyl	CO	3.63 ± 0.1
38	4-trifluoromethyl-2-hydroxyphenyl	CO	47 %

1
2
3
4
5
6
7
8
9
10
11
12
13
14
15
16
17
18
19
20
21
22
23
24
25
26
27
28
29
30
31
32
33
34
35
36
37
38
39
40
41
42
43
44
45
46
47
48
49
50
51
52
53
54
55
56
57
58
59
60

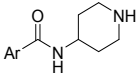
39	4-fluoro-2-hydroxyphenyl	CO	NI
40	1-hydroxy-2-naphthyl	CO	6.90 ± 0.24
41	2-hydroxy-1-naphthyl	CO	NI
42	3-hydroxy-2-naphthyl	CO	1.57 ± 0.03
43	2-naphthyl	CO	19.81 %
44	1-indolyl	CO	NI
45	4-oxo-3-quinolyl	CO	NI
46	2-pyridin-3-ol	CO	8.86%
47	6-methoxy-1-hydroxy-2-naphthyl	CO	7.18 ± 0.33
Compound	Ar	% Inhibition at 10 µM	
			
53	1-hydroxy-2-naphthyl		NI

Table 1: Efficacy of *para*-aminobenzyl compounds towards KLK6. For each compound, the inhibitory effect was quantified either by the percentage inhibition of KLK6 at 10 μ M, or by the IC_{50} for compound hits. To determine the IC_{50} , compounds at different concentrations (concentration ranges adjusted depending of the inhibitory potency) are pre-incubated 15 minutes at 37°C with KLK6 (2 nM). The enzymatic reaction is triggered by the addition of the Boc-QAR-AMC substrate (100 μ M) in 50mM Tris buffer, 1M Citrate 0.05% Brij-35; pH 7.4 at 37 °C. NA: not applicable. NI: non-inhibitor. The data result from at least three independent experiments in duplicate. The IC_{50} values were calculated by fitting the experimental data to eq. 2a or eq.2b and expressed as geometric standard deviation.

Then, we assessed inhibitory potency of our hit compounds (**32**, **37**, **40**, **42** and **47**) and of reference compound **28** towards KLK1 and plasmin, as these two proteases are thought to be part of the proteolytic network of KLK6 in MS.¹⁹ All these *para*-aminobenzyl derivatives lead to at least 50% inhibition of the plasmin activity except inhibitor **28** (45%) while all the tested inhibitors lead to an inhibition of at least 50% of KLK1 activity at a concentration of 10 μ M (data not shown). The inhibitory potency (IC_{50}) of hit compounds was then determined. The IC_{50} values with respect to plasmin place compound **47** (IC_{50} =3.3 μ M) at the top while reference compound **28** (IC_{50} =21.3 μ M) has one of the lowest efficiency (**Table 2**). At the same time, compound **42** is characterized by and IC_{50} value of 5.1 μ M towards KLK1, while other compounds showed lower inhibitory potency and were thus not selected for further mechanistic studies (**Table 2**).

1
2
3
4
5
6
7
8
9
10
11
12
13
14
15
16
17
18
19
20
21
22
23
24
25
26
27
28
29
30
31
32
33
34
35
36
37
38
39
40
41
42
43
44
45
46
47
48
49
50
51
52
53
54
55
56
57
58
59
60

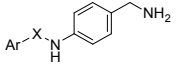
			IC₅₀ (μM)	
Compound	Ar	X	Plasmin	KLK1
28	5- <i>tert</i> -butyl-2-hydroxyphenyl	CO	21.3 ± 3.6	38.6 ± 1.9
32	4-methyl-2-Hydroxyphenyl	CO	9.2 ± 0.6	26.3 ± 1.1
37	4-isopropyl-2-Hydroxyphenyl	CO	4.8 ± 0.2	8.4 ± 0.3
40	1-hydroxy-2-Naphthyl	CO	10.2 ± 0.6	21.3 ± 1.6
42	3-hydroxy-2-Naphthyl	CO	7.4 ± 0.6	5.1 ± 0.2
47	6-methoxy-1-hydroxy-2-naphthyl	CO	3.3 ± 0.2	16.1 ± 0.4
49	7-methyl-1-hydroxy-2-naphthyl	CO	6.7 ± 0.6	49.4 ± 4

Table 2: Efficacy of KLK6 *para*-amino benzyl hit inhibitors on Plasmin and KLK1. For each compound, the inhibitory effect was quantified by the IC₅₀. To determine the IC₅₀, compounds at different concentrations (from 100 to 1.56 μM) are pre-incubated 15 minutes at 37°C with Plasmin (3 nM) or KLK1 (0,75 nM) in 50mM Tris buffer, 1M Citrate 0.05% Brij-35; pH 7.4 at 37 °C. The enzymatic reaction is then triggered by the addition of the Boc-QAR-AMC substrate (100 μM) for Plasmin and H-PFR-AMC substrate (100 μM) for KLK1. The data result from at least three independent experiments in duplicate. The IC₅₀ values were calculated by fitting the experimental data to eq. 2a or eq.2b and expressed as geometric standard deviation.

Hit compounds (**32**, **37**, **40**, **42**, **47**, **49**) and reference compound **28** were assessed by the evaluation of their selectivity spectrum against a set serine proteases and proteases involved in CNS homeostasis. **Table 3** provides an overview of putative cross-inhibition within a large set of proteases both serine proteases challenging in the CNS (KLK8, tPA, thrombin, trypsin, trypsin 3, KLK11) but also other kallikreins (KLK3, KLK4, KLK5, KLK14), matriptase, and diverse

proteases involved in CNS inflammation (Caspase-2, Caspase-3, Caspase-6, Cathepsin L). Overall, this screening shows that hit compounds **32** and **42** have little effect on these selected challenging proteases in contrast to the other identified inhibitors (**28**, **37**, **40**, **47**, **49**) that display significant inhibition on several proteases. This allows to conclude that compounds **32** and **42** are quite specific to KLK6 and its proximal proteolytic network.

<i>Inhibitor</i> <i>Protease</i>	28	32	37	40	42	47	49
KLK4	0	0	45	14	2	3	6
KLK5	35	5	24	22	4	31	0
KLK7	9	12	7	0	6	10	11
KLK8*	16	34	58	22	61	45	53
KLK11*	56	39	75	80	45	0	88
KLK13	5	10	15	2	19	0	12
KLK14	1.5	3	12	11	5	16	4
Caspase-2*	5	0	15	30	4	14	8
Caspase-3	11	0	13	10	5	3	10
Caspase-6*	13	5	12	56	40	70	31
Cathepsin L*	20	32	1	30	25	28	27
Matriptase	0	0	13	29	8	37	0
Thrombin	2	0	32	5	0	6	6
tPA	11	0	6	18	6	10	9
Trypsin	5	15	91	34	25	41	32
Trypsin 3*	15	20	73	30	36	32	21

Table 3: Selectivity of the inhibition of hit compounds toward selected CNS concurrent proteases (Inhibition percentage at 10 μ M, %). Each inhibitor (10 μ M) is preincubated with the enzyme at the optimal concentration for 15 minutes at 37°C. The reaction is triggered by the addition of the specific AMC-substrate in the appropriate buffer (cf section “Material and Methods – Selectivity profiling”). The data result from at least three independent experiments with a standard deviation < 10%. * **Proteases implicated in the CNS physiological processes. Gray light: significative percentage of inhibition.**

Mechanism of inhibition: hit compounds

Mechanistic studies were only performed for hit compound that display an ideal balance between potency and selectivity profiles towards KLK6 and its proximal proteolytic network (KLK1 and Plasmin) as well as the reference compound **28** for comparison. The reversibility of the inhibitions exerted by the compounds on KLK6 and its proteolytic network (Plasmin and KLK1) were demonstrated by the dilution method as described in the "Materials and methods" section. This experiment distinguishes an irreversible covalent inhibitor from a reversible one. Whatever the compound tested, a 1/100 dilution of the enzyme-inhibitor complex allowed restoring the initial activity of KLK6 to more than 80%. Hence, hit compounds are reversible inhibitors (**Figure 2**). The mechanisms were determined using representations of Dixon for hits and reference compounds. The results are shown in **Figure 2**. The Dixon graphs obtained for compounds **28**, **32** and **40** (**Figures 2A**, **2B** and **2C**) are typical of competitive inhibitors. Compounds **28**, **32** and **40** have K_i values of 4.3 μ M, 2 μ M and 2.4 μ M, respectively. Surprisingly the mechanistic profile of compound **42** was found compatible with a noncompetitive inhibition with a K_i value of 0.8 μ M which may be indicative of a more complex binding (**Figures 2D**). The Dixon plots for compounds **37** and **47** are provided in the supplementary data section (**Figure S1**).

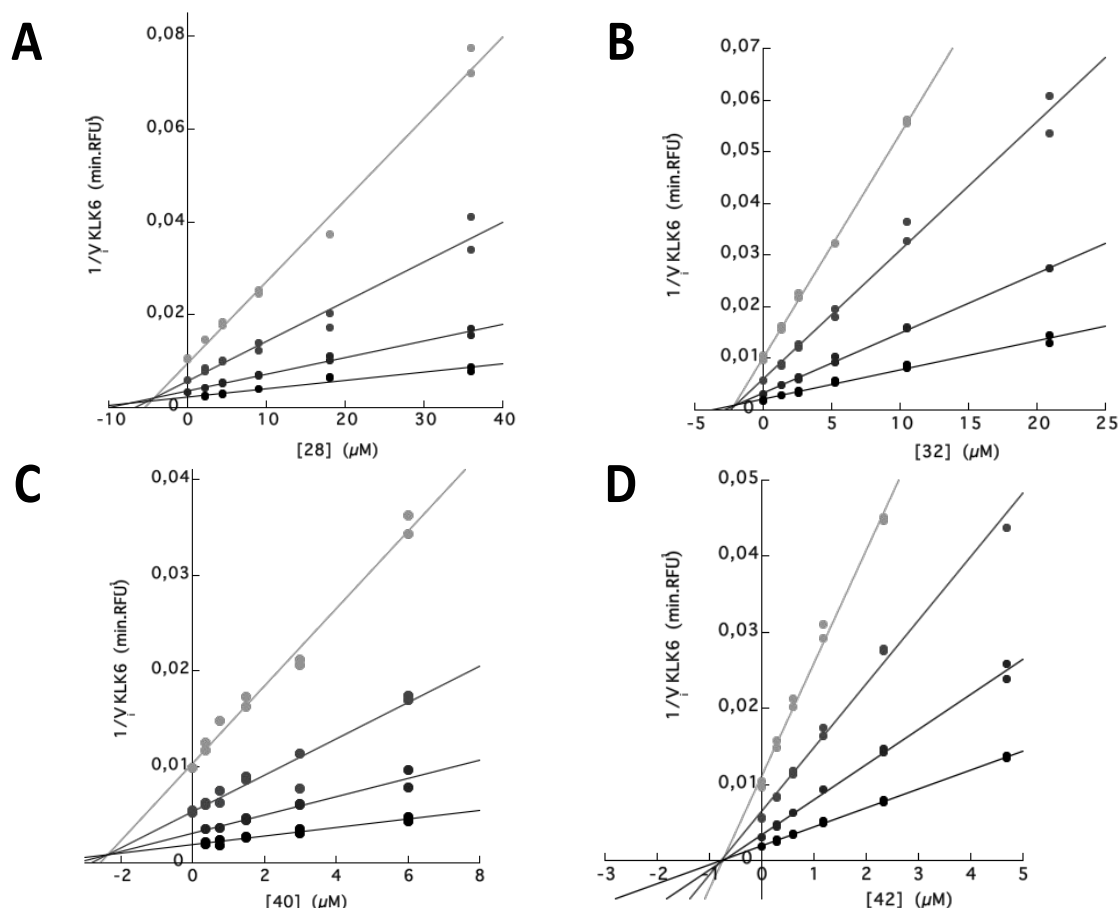


Figure 2: Mechanisms of inhibition towards KLK6. Dixon plots for inhibitors **28** (A), **32** (B), **40** (C) and **42** (D). Inhibitors at different concentrations (1/4; 1/2; 1; 2; 4 of the IC_{50} value) were tested using 2 nM KLK6 with substrate Boc-QAR-AMC at different concentrations (125; 62.5; 31.25; 15.625 μ M) in 50 mM Tris, 1 M Citrate, 0.05% Brij-35, pH 7 buffer at 37 °C.

Concerning plasmin and KLK1, all compounds are reversible inhibitors as shown using the dilution method. Dixon plots obtained for compounds **28**, **40** and **42** (Figures 3A, 3B and 3C) are typical of competitive inhibitors towards plasmin. Compounds **28**, **40** and **42** have K_i values of 14.5 μ M, 1.5 μ M and 1.3 μ M respectively. The Dixon plot for KLK1 obtained with inhibitor **42** is also typical of a competitive inhibitor ($K_i=2.4$ μ M) (Figure 3D and Table 4). Hence, it is shown that some of our hit KLK6 inhibitors also target key serine proteases of KLK6 proteolytic network with a relatively good affinity, which may constitute interesting perspective for a polypharmacological strategy.

Compound	KLK6		Plasmin		KLK1	
	Type of inhibition	K _i (μM)	Type of inhibition	K _i (μM)	Type of inhibition	K _i (μM)
28	Competitive	4.3 ± 1.6	Competitive	14.5 ± 1.2	NA	NA
32	Competitive	2 ± 0.5	NA	NA	NA	NA
37	Competitive	1.5 ± 0.2	NA	NA	NA	NA
40	Competitive	2.4 ± 0.1	Competitive	1.5 ± 0.5	NA	NA

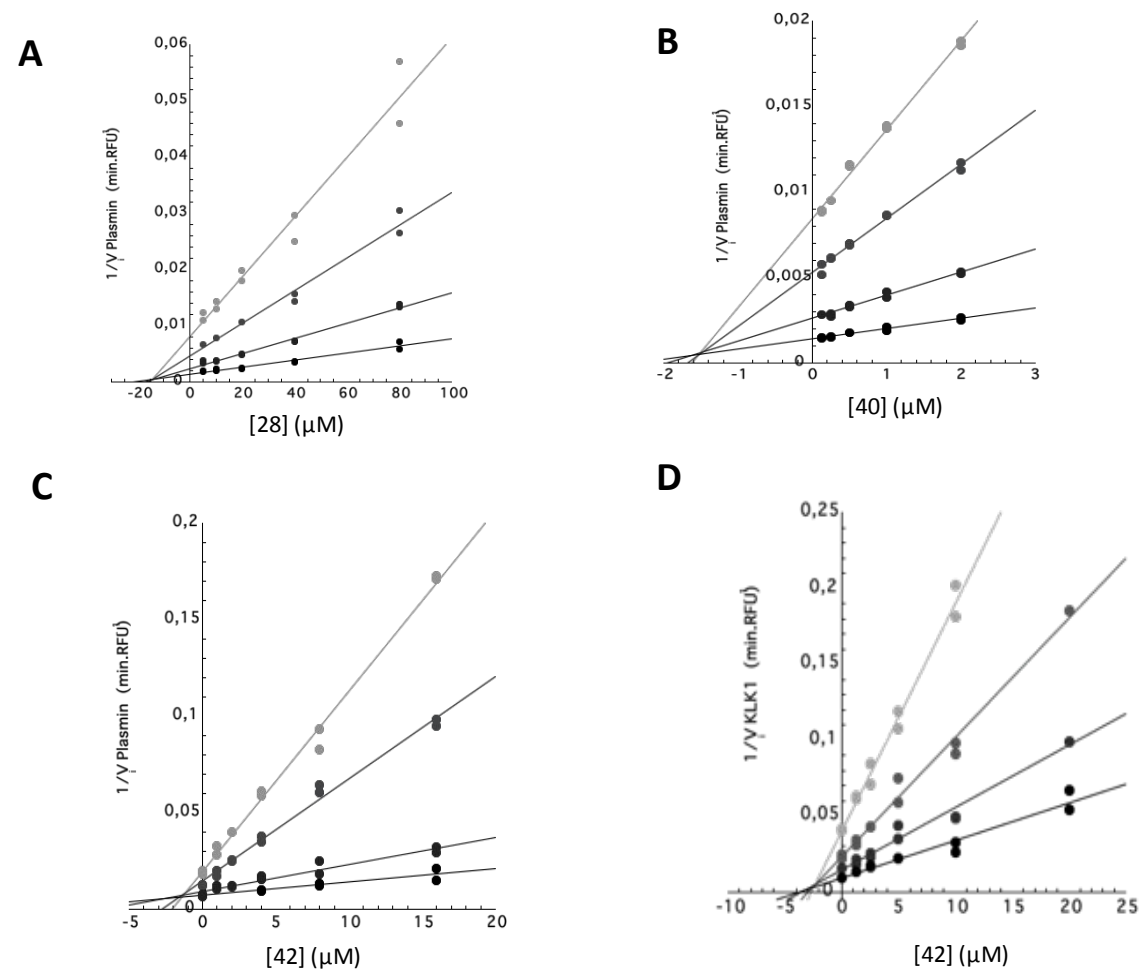


Figure 3: Mechanisms of inhibition towards KLK1 and plasmin. (A-C) Dixon plots for inhibitors **28** (A), **40** (B), **42** (C) towards plasmin. **(D)** Dixon plot for inhibitor **42** towards KLK1. Inhibitors at concentrations (1/4; 1/2; 1; 2; 4 of the IC₅₀ value) were tested on plasmin (3 nM) or KLK1 (0,75 nM) with respectively Boc-QAR-AMC or H-PFR-AMC substrates at concentrations (125; 62.5; 31.25; 15.625 μM) in 50 mM Tris buffer, 1 M Citrate, 0.05% Brij-35, pH 7 at 37 °C.

42	Non-competitive	0.8 ± 0.3	Competitive	1.3 ± 0.53	Competitive	2.4 ± 0.5
47	Competitive	$1 \pm 0,3$	NA	NA	NA	NA

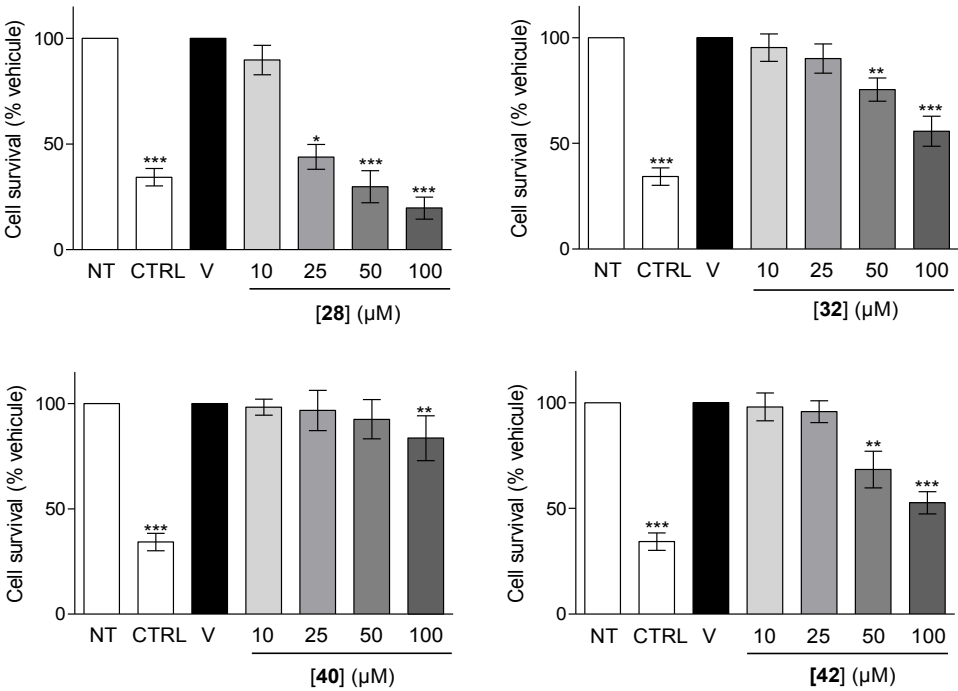
Table 4: Mechanisms of inhibition and K_i values of hit compounds on KLK6 and its associated proteolytic network (KLK1 and plasmin). NA, not applicable

Evaluation of the cytotoxicity of hit compounds toward neural cells

To ensure that hit compounds (**32**, **40** and **42**) may constitute good starting points for further applications, their potential cytotoxicity toward neural cells was first evaluated in comparison to reference compound **28** on primary cultures of mouse cortical and striatal neurons at 10, 25, 50 and 100 μM (**Figure 4A**). Compounds **32** and **42** showed similar effects on both cortical and striatal neurons. A slight effect is observed from a concentration of 50 μM of inhibitors **32** and **42**, with percentages of cell survival around 65-70%. In contrast, compound **40** is the only compound showing a cytotoxic effect on striatal neurons from a concentration of 10 μM , this cytotoxicity is stable over the concentration range meaning that a plateau may be reached (**Figure 4B**). Thus, these newly identified inhibitors are all very poorly cytotoxic in comparison with the reference inhibitor **28**, which displays a noticeable cytotoxic effect, even at 25 μM , very close to the treatment with rotenone vehicle at 50 μM .

Hence, since compounds **32**, **40** and **42** did not show toxic effects towards neurons, they were selected for further studies in oligodendrocyte precursor cell (OPC) cultures as relevant biological model for MS.

A



B

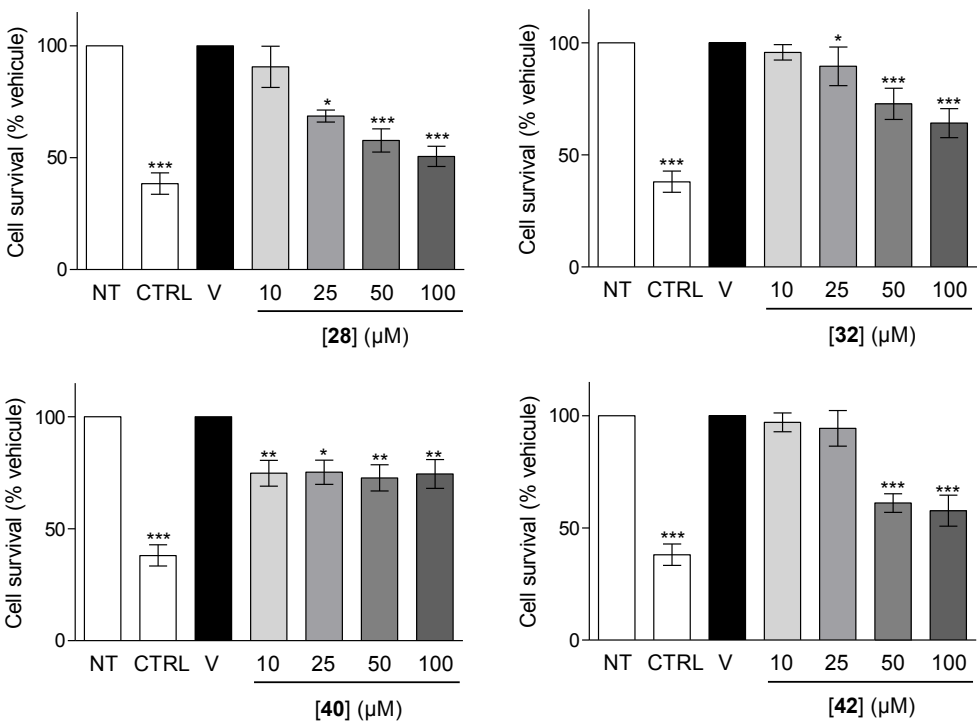


Figure 4: Cytotoxicity of hit inhibitors (32, 40 and 42) and reference compound 28 against primary cultures of cortical and striatal neurons. A – Cortical neurons. B- Striatal neurons. Primary cultures were treated either with inhibitors in a concentration range from 10 μM to 100 μM or with the vehicle (DMSO 1%, “V”) or with rotenone 50 μM (CTRL) for 24 hours (N=3). Cell survival was then measured using XTT assay. All data sets were compared to the vehicle condition (V) for the generation of the p-values. * p-value < 0.05; ** p-value < 0.01; *** p-value < 0.001 (Kruskal-Wallis test). NT: no treatment

Pro-differentiating effect of hit compounds

Oligodendrocytes are derived from OPCs, a class of progenitors highly abundant during development but also persistent in the adult CNS, where they contribute to myelin remodelling and remyelination following acute demyelination. Although efficient remyelination occurs in the early stages of MS, it becomes inefficient and ultimately fails with disease progression. Remyelination requires the generation of new mature oligodendrocytes (OLs) from OPCs that must be recruited to the demyelinated lesions. Over the last decade, there have been huge interest in developing medicines to improve remyelination in MS.³⁴ The approaches range widely, from developing novel medicines and repurposing existing drugs. We thus assayed hit compounds on CG4 cell line and rat OPC primary cultures to check for their ability to induce differentiation. To monitor OPC differentiation, we developed a stable CG4 cell line expressing the GFP reporter at all stages of the oligodendroglial lineage cells and the mCherry reporter only in mature oligodendrocytes (**Figure 5A**). This innovative cellular assay allows the screening of promyelinating compounds based on the detection of fluorescence parameters. Indeed, both morphological changes and generation of mature oligodendrocytes can be monitored in a single assay, based on EGFP and mCherry fluorescence, respectively. After few days in basal medium, CG4 cells start to differentiate and expressed mCherry (**Figure 5B, 5C**). Fluorescence imaging (90 image fields were acquired for each condition) and quantification were performed with the Arrayscan XTI Imaging System. For each concentration tested, we quantified the number of mCherry+ cells and data were normalized relatively to control (N1 basal medium). 9cis retinoic acid (9cis-RA), a well-known compound promoting OPC differentiation was used a positive control.⁵³

Our data revealed no statistically significant change in the number of mCherry+ cells after treatments with compounds **40** (**Figure 5F**). For compound **28**, a significant increase of the

1
2
3
4
5
6
7
8
9
10
11
12
13
14
15
16
17
18
19
20
21
22
23
24
25
26
27
28
29
30
31
32
33
34
35
36
37
38
39
40
41
42
43
44
45
46
47
48
49
50
51
52
53
54
55
56
57
58
59
60

number of mCherry+ oligodendrocytes was observed at 2μM, while treatments at higher concentrations ranging from 10 μM to 30 μM lead to a complete loss of cells (**Figure 5D**), presumably due a cytotoxicity. In contrast, for compound **32** (**Figure 5E**) a significant increase of differentiation was observed with respect to basal control at concentrations of 6 μM ($p \leq 0.05$) and 8 μM ($p \leq 0.01$, Mann-Whitney test), and for compound **42** (**Figure 5G**) at 5 μM ($p \leq 0.05$, Mann-Whitney test). Thus, compounds **32** and **42** promote the differentiation of CG4 cells into mature oligodendrocytes. In view of their pharmacological and biological profiles, compounds **32** and **42** appear particularly suitable. Compounds **32** and **42** were also evaluated on primary cultures of rat OPCs (**Figure 6**). In this model, the differentiation rate was measured by the quantification of the number of MBP-expressing oligodendrocytes. MBP is a major constituent of myelin and is commonly used as a marker of mature oligodendrocytes. Compounds **32** and **42** promote the differentiation at concentrations of 8 μM and 5 μM, respectively. Overall, these findings support the pro-myelinating potential of *para*-aminobenzyl-hit derivatives.

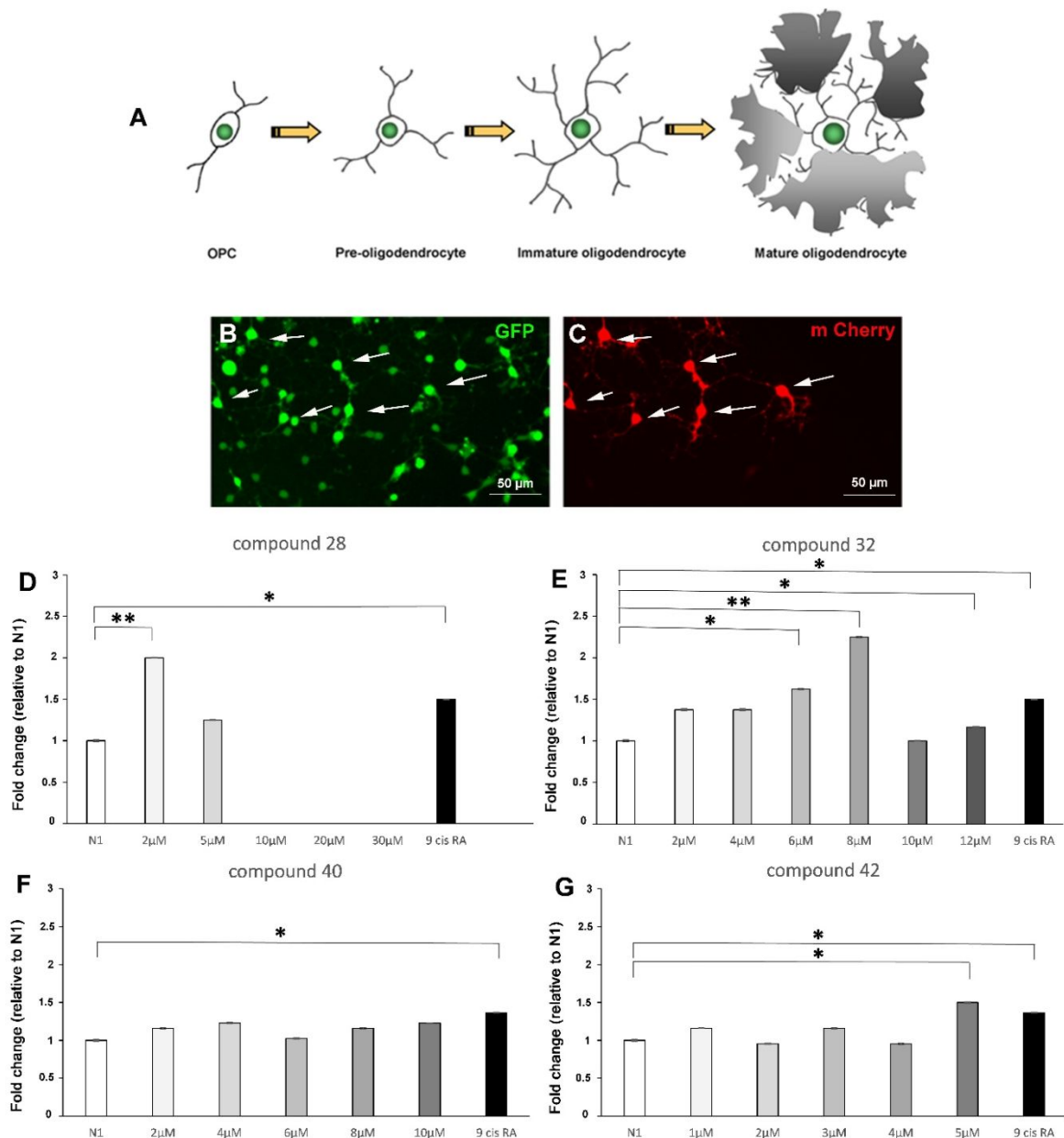


Figure 5: KLK6 inhibitors promote oligodendrocyte differentiation on the CG4 mCherry/GFP cell line.

Schematic representation of the different developmental stages of the CG4 cell line (A). Differentiation of the mCherry/GFP double fluorescent CG4 cell line, after 4 days of differentiation in basal medium (B-C). GFP fluorescence is shown in (B) and mCherry fluorescence in (C). Note that the differentiation of CG4 cells is not synchronous in these cultures and the expression of mCherry occurs specifically at the mature oligodendrocyte stage. Graphs of the fold change of the number of mCherry+ cells in N1 alone, N1 + compound **28** (D), N1 + compound **32** (E), N1 + compound **40** (F) or N1 + compound **42** (G), after 4 days of differentiation. The treatment with KLK6 inhibitors **32** and **42** induces a significant increase of CG4 cell differentiation at 8 μ M and 5 μ M respectively, relative to the N1 basal medium. Note that CG4 cells treated with compound **28** at 2 μ M lead to a significant increase of the number of mCherry+ oligodendrocytes. However, at higher concentrations with this compound (ranging from 10 to 30 μ M), cells were lost presumably due to a cytotoxicity. Wilcoxon - Mann Whitney test: * $p \leq 0.05$, ** $p \leq 0.01$. 9 cis retinoic acid (9cis-RA, 1 μ M) was used as a positive control. Scale bar (B, C): 50 μ m.

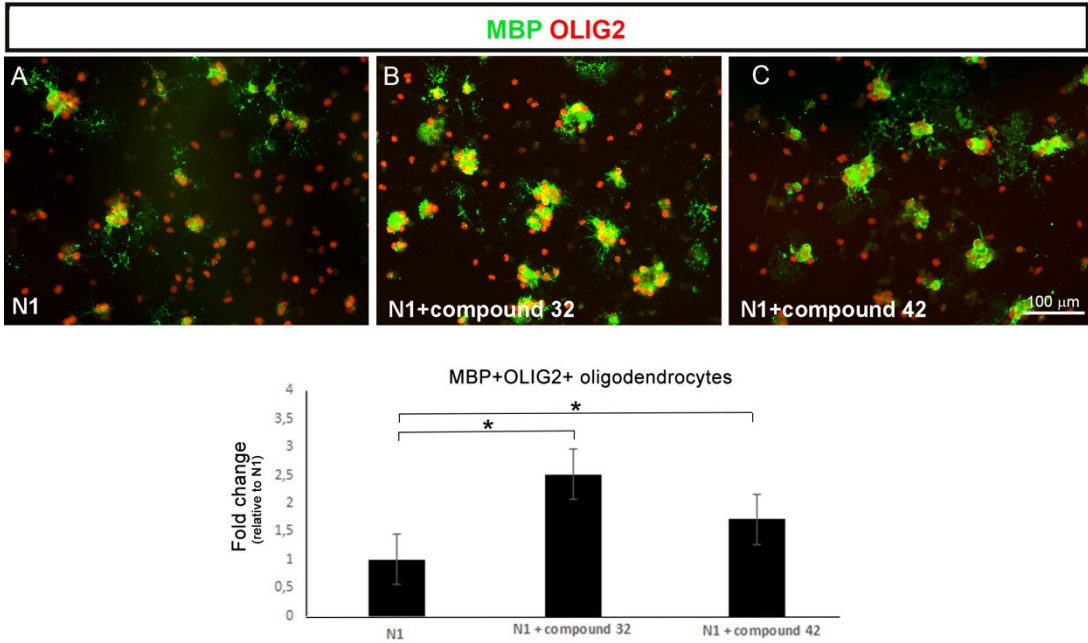


Figure 6: KLK6 inhibitors promote oligodendrocyte differentiation of primary OPC cultures. Primary OPC cultures, stained for MBP (green) and Olig2 (red), after 4 days of differentiation in basal medium (A), in the presence of compound **42** (B, 5µM) or compound **32** (C, 8µM). The treatment with KLK6 inhibitors induces a significant increase of MBP+ oligodendrocytes with respect to control. N=3 independent experiments; Wilcoxon - Mann Whitney test: *p ≤ 0.05). Scale bar (A, B, C): 100µm.

Anti-inflammatory properties of hit compounds

In MS, chronic activation of microglia may contribute to neurodegeneration and neuroinflammation. ³⁵ Thus, we also examined the impact of hit compounds **32** and **42** on microglial activation and pro-inflammatory cytokines. These experiments were carried in primary microglial cells isolated from newborn rat brain. ³⁶ Effects of selected compounds on microglia were analyzed after treatment with lipopolysaccharide (LPS, 10 ng/ml) alone or in presence of different concentrations framing IC₅₀ values of compounds **32** and **42**, using dexamethasone as positive control (**Figure 7**). Using quantitative RT-qPCR of pro- and anti-inflammatory cytokine gene expression, we showed that compound **42** significantly lowered the expression of TNFα and IL1β pro-inflammatory cytokines while compound **32** had no

effect. This result illustrates potential distinct dual therapeutical effects and/or mechanism of action for these hit compounds.

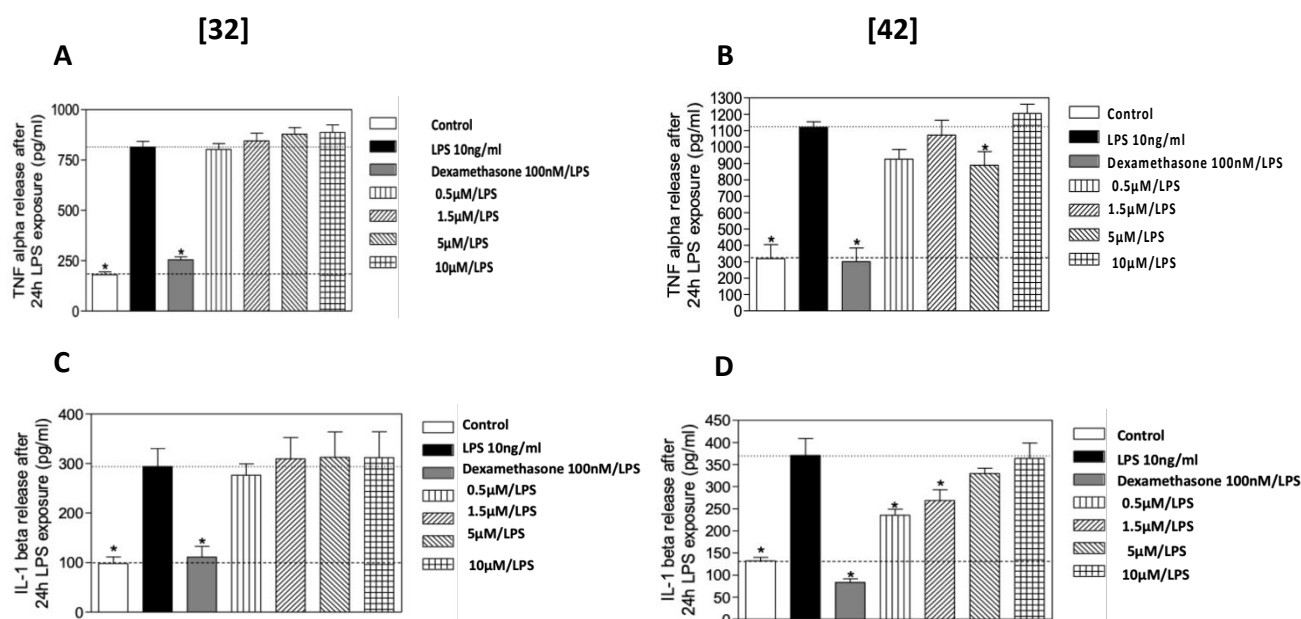


Figure 7: Anti-inflammatory potential of KLK6 inhibitors on a primary culture of microglia. Changes in TNF- α (A-B) and IL-1 β (C-D) secretions after 24 hours of LPS exposure (10 ng. mL⁻¹) and treatment by either inhibitor **32** (left) or **42** (right) in the concentration range [0,5 μ M – 10 μ M]. Cytokine secretion was measured by ELISA assay. The treatment with inhibitor **42** induces a significant decrease of TNF α and IL1- β secretions. Control: No treatment. Dexamethasone (100 nM): positive control (n=3). (graph, * p \leq 0.05)

Molecular docking modelling to study structural basis of the inhibition

In silico analyzes using molecular docking with the AutoDock Vina software highlighted some characteristic structural bases on the inhibition of hit compounds **42** and **32** (Figure 8A). Figures 8B and 8C illustrates their positioning for the best docking poses. Overall, the orientation of both compounds within the active site is identical with the benzylamine group pointing to the S1 pocket and the phenol/naphthol groups to the catalytic triad. Inhibitors **32** (Figure 8B) and **42** (Figure 8A) share several polar contacts with some active site residues, namely H57 and S195. In particular, the NH of the amide bond of compound **32** establishes a

1
2
3 direct H-bond with the catalytic S195. We do not exclude a certain flexibility in this region,
4
5 given the obtained results, which could allow the NH of the amide bond of compound **42** to
6
7 behave similarly, this behavior may in part explain the non-competitive mechanism
8
9 underlined by Dixon plots. The OH hydroxyl group of phenols or naphthols could also
10
11 contribute to a polar bond with Q192 side chain as well as the NH backbone of G193. Finally,
12
13 the primary amine shows strong polar contact in both cases with D189 and S190 side chains
14
15 and with W215 backbone. The visual inspection of other docking poses with lower scores
16
17 informed us about the certain degree of freedom of the benzylamine moiety inside the S1
18
19 pocket, the benzyl group having enough space to slightly rotate around its axis, even
20
21 suggested by the two best poses of compounds **32** and **42**. These poses are quite compatible
22
23 with their mechanism of inhibition.
24
25
26
27
28
29
30
31
32
33
34
35
36
37
38
39
40
41
42
43
44
45
46
47
48
49
50
51
52
53
54
55
56
57
58
59
60

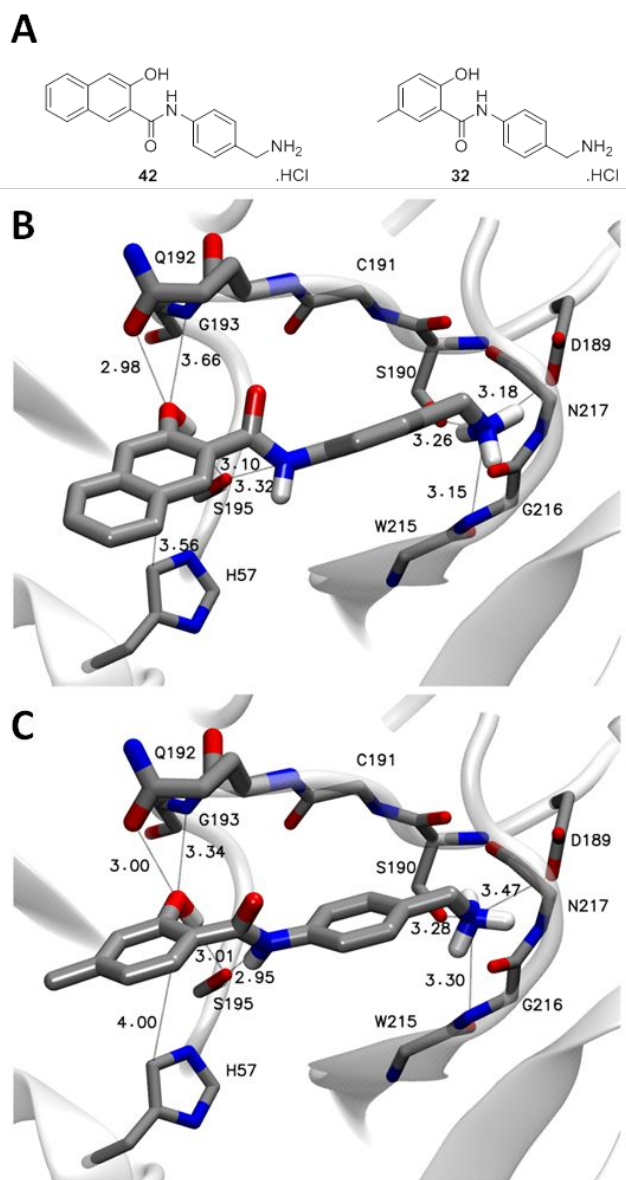


Figure 8: Structure of lead compounds **42** and **32** (A) and pose predictions by molecular docking of **42** (B) and **32** (C) in KLK6. Most relevant interactions were depicted by dashed lines together with distances in Angström. Compounds as well as residues of the proteins mainly involved in ligand interactions are shown in licorice while the full proteins are shown in transparent-white cartoon. The color code for the atoms is as follows: Carbon in grey, Oxygen in red, Nitrogen in blue and Hydrogen in white. The side chains which make no contact with **42** and **32**, as well as hydrogens of the protein and non-polar hydrogens of **42** and **32** were not represented for clarity.

1
2
3
4
5
6
7
8
9
10
11
12
13
14
15
16
17
18
19
20
21
22
23
24
25
26
27
28
29
30
31
32
33
34
35
36
37
38
39
40
41
42
43
44
45
46
47
48
49
50
51
52
53
54
55
56
57
58
59
60

Pharmacological profile and evaluation of drug-like properties

To gain more insights on the drug-like potential of the two selected hit compounds, different evaluations were performed to assess their: i) their putative effect of on coagulation; iii) their cross-reactivity toward key pharmacological targets using the SafetyScreen44™ Panel from Eurofins ³⁷; iv) some ADME-Tox properties: solution properties (aqueous solubility in simulated fluids and plasma protein binding), *in vitro* absorption (Caco2 cell line); *in vitro* metabolism (intrinsic clearance using human liver microsomes). More relevant parameters are summarized in Supplementary Data, **Table S2**. Altogether, these evaluations demonstrated that hit compounds **32** and **42** bear a very favorable pharmacological profile. They were shown to have no toxicity on coagulation after incubation with human blood (neither the activated partial thromboplastin time nor the prothrombin ratio were modified) and to possess acceptable aqueous solubility (> 150 μM, except for **42** at pH≥ 7.4), permeability (> 90%) and clearance properties (half-life >120 min) when compared to reference substances. Interestingly, among the 44 screened targets both receptors and enzymes, very few were inhibited by our lead compounds. No activity at ion channels (including hERG) was detected meaning weak toxicity. The only significant detected off targets were of interest both for CNS diseases (5-HT_{2A/2B} serotonin receptors) or inflammation (COX-2). ³⁸ Hence, the selected compounds display favorable drug-like properties and constitute thus excellent starting point to derive drugs for regenerative therapy of MS and related-diseases associated with a deregulation of KLK6 and proximal proteolytic network.

Conclusion

Current MS therapeutics are mainly immuno- modulatory, having very few effect on neuroregeneration of damaged CNS tissue; they are thus primarily effective at the acute stage of disease, but much less so at the chronic stage. An MS therapy that has both immunomodulatory and neuro- regenerative effects would be highly beneficial. Novel targets aiming to promote such therapeutic strategies are thus of great interest. ⁸ KLK6 and its proximal proteolytic network may constitute a new opportunity to develop new therapeutics or molecular tools for MS physiopathology. A series of *para*-aminobenzyl derivatives incorporating a phenol or a naphthol group was thus designed, synthesized and studied for their properties to inhibit KLK6 activity and proteases that may be involved into the KLK6's pathological network in MS, namely inhibitions of both KLK1 and plasmin may be interesting in a polypharmacological perspective.

Several designed low molecular weight inhibitors are low-micromolar potency and reversible towards KLK6. In the phenol series, introduction of an alkyl group at the C4 position led to more potent compounds (**32** and **37**), whereas in the naphthol series, the best activity was obtained with the 1- and 3-naphthol derivatives (**40** and **42**). Interestingly, these hit compounds were selective of KLK6 and its associated network over a large set of CNS concurrent proteases, and devoid of cytotoxic effects on primary cultures of mouse cortical and striatal neurons and oligodendrocytes. Most importantly, we show for the first time that synthetic inhibitors of KLK6 and proximal proteolytic network, a key actor of MS physiopathology, are able to promote the differentiation of OPCs into mature oligodendrocytes *in vitro*, which is as far as we know the first report of such properties. Indeed, the presence of oligodendrocyte progenitors (OPCs) in the adult CNS, which are able to migrate and regenerate remyelinating oligodendrocytes in demyelinating lesions, represent

the main cellular target for the development of pharmacological strategy aiming to promote remyelination. In line with this idea, compounds **32** and **42** were also tested for their potential effect on neuroinflammation using primary cultures of microglia. Compound **42** decreased significantly the expression of pro-inflammatory cytokines. Hence, compound **42** in contrast to compound **32** appears to be a good candidate as a first-in-class KLK6 inhibitor bearing both remyelinating and anti-inflammatory potentials. There is a growing interest to decipher mechanisms regulating OPC differentiation for the identification of novel specific pharmacological targets for remyelination-enhancing therapy.³⁴ In another hand, there also a growing interest for pro-differentiating compounds selected first through screening campaigns and more recently using rational design as illustrated in up-to-date reports. Namely, spiroindolines were shown as novel inducers of OPC differentiation.³⁹ Recently, benzothiazoles LRRK2 inhibitors were shown to promote OPC proliferation and differentiation through Wnt/ β -catenin signaling pathway.⁴⁰ Moreover, modified flavonoids were reported as selective inhibitors of hyaluronidase activity and could promote OPC maturation, making them excellent candidates to accelerate myelination or promote remyelination following perinatal and adult CNS insults.⁴¹ Thus, in view of their pharmacological and biological properties, *para*-aminobenzylamine derivatives **32** and **42** appear particularly valuable starting points for the development of original pharmacological strategies aiming to promote remyelination in demyelinating diseases, such as MS.

Experimental section

All reagents were analytical grade. Distilled water was filtered and deionized through a Millipore water purification system.

Chemistry Materials and General Procedures

Commercially available reagents and solvents were used without further purification. Reactions were monitored by an analytical Waters Alliance 2690 HPLC instrument, equipped with a photodiode array and an analytical Chromolith Speed Rod RP-C18 185 Pm column (50 x 4.6 mm, 5 mm), at a flow rate of 3.0 mL/min, and gradients of 100/0 to 0/100 eluents A/B for 5 min (eluent A = H₂O/0.1% TFA and B = CH₃CN/0.1% TFA). Detection was performed at 214 nm. ¹H and ¹³C NMR spectra were recorded on Bruker spectrometers (300 or 400 MHz) at room temperature in deuterated solvents. Chemical shifts (δ) are expressed in parts per million (ppm), relative to the resonance of CDCl₃ = 7.26 ppm for ¹H (77.16 ppm for ¹³C), CD₃OD = 3.31 ppm for ¹H (49.00 ppm for ¹³C) or DMSO d₆ = 2.50 ppm for ¹H (39.52 ppm for ¹³C). The following abbreviations were used: s (singlet), d (doublet), t (triplet), q (quartet), m (multiplet), bs (broad singlet). Analytical thin-layer chromatography (TLC) was carried out on aluminum plates covered with 0.2 mm of silica and column chromatography was performed on silica gel 60 (70-230 mesh).

The LC/MS system consisted of a Waters Alliance 2695 HPLC, coupled to a Micromass (Manchester, UK) ZQ spectrometer (positive electrospray ionization mode, ESI+). All the analyses were carried out using a Merck Chromolith Speed rod C18, 25 x 4.6 mm reversed-phase column. A flow rate of 3mL/min and a gradient of (0–100) % B over 3 min (or over 15 min) were used. Eluent A: water/0.1% HCO₂H; eluent B: acetonitrile/0.1% HCO₂H. Retention

times (RT) are given in minutes. Nitrogen was used for both the nebulizing and drying gas. The data were obtained in a scan mode ranging from 100 to 1000 m/z in 0.1 s intervals; 10 scans were summed up to get the final spectrum. High-resolution mass spectrometry analyses were performed with a Waters Synapt G2-S time-of-flight mass spectrometer fitted with an electrospray ionisation source. All measurements were performed in the positive ion mode. Melting points (Mp) are uncorrected and were recorded on a Stuart capillary melting point apparatus SMP3. All compounds tested for biological activity showed >95% purity, as assessed by RP-HPLC (Chromolith Speed Rod RP-C18 185 Pm column 50×4.6 mm, $5 \mu\text{m}$; flow rate: 5.0 mL/min; gradients from 100/0 to 0/100 eluents A/B over 5 min, in which eluent A = $\text{H}_2\text{O}/0.1\%$ TFA and B = $\text{CH}_3\text{CN}/0.1\%$ TFA; detection was done at 214 nm).

Compound **26** was synthesized according to the procedure described by Darensburg et al.⁴² and its physical characteristics were in agreement with the published data. Carboxylic acids were commercially available or synthesized according to the procedures described in ESI.

Synthesis of *tert*-butyl (4-nitrobenzyl) carbamate (**1**):

To a solution of 4-nitrobenzylamine hydrochloride (1 g, 5.3 mmol) in 10 mL of dichloromethane were added 480 μL of triethylamine (348 mg, 3.44 mmol, 1.3 equiv.) and 790 μL of *tert*-butyl dicarbonate (751 mg, 3.44 mmol, 1.3 equiv.). The solution was stirred at room temperature for 2 hours. Then was added 0.3 equiv. of aminomethyl polystyrene resin and the suspension was stirred for 1 hour. After filtration, the solution was washed with 1M aqueous potassium hydrogensulfate solution (2x 15 mL) and with brine (15 mL). The organic layer was dried over Na_2SO_4 , filtered and the solvent is evaporated *in vacuo* to offer compound **1** as a white solid (m= 1.06 g, 80% yield); mp 109-111°C (lit. 109-110°C)⁴³; ^1H NMR (CDCl_3 , 300 MHz): δ ppm 1.43 (s, 9H), 4.37 (d, 2H, $J = 6.2$ Hz), 5.03 (bs, 1H), 7.41 (d, 2H, $J = 8.8$ Hz), 8.14 (d,

2H, $J = 8.8$ Hz); ^{13}C NMR (CDCl_3 , 75 MHz): δ ppm 27.5, 44.2, 85.3, 123.9, 127.9, 146.9, 147.4, 156.0; HPLC, RT= 1.68 min.

Synthesis of *tert*-butyl (4-aminobenzyl)carbamate (**2**):

To a solution of compound **1** (1 g, 4.0 mmol) in 20 mL of ethyl acetate was added 10% palladium activated on charcoal (~20 mg). The suspension was hydrogenated at atmospheric pressure for 4 hours at room temperature. The suspension was then filtered on celite and the filtrate was evaporated under reduce pressure to yield compound **2** as a pale orange solid, m = 880 mg, quantitative yield. Mp 72-75°C (lit. 72-75°C)⁴⁴; ^1H NMR (CDCl_3 , 300 MHz): δ ppm 1.43 (s, 9H), 3.60 (bs, 2H), 4.14 (d, 2H, $J = 5.6$ Hz), 4.74 (bs, 1H), 6.60 (d, 2H, $J = 8.4$ Hz), 7.02 (d, 2H, $J = 8.4$ Hz); ^{13}C NMR (CDCl_3 , 75 MHz): δ ppm 28.5, 44.5, 79.4, 115.3, 128.9, 135.1, 145.8, 155.9; HPLC, RT= 0.93 min; MS (ESI+): m/z 223.3 $[\text{M}+\text{H}]^+$.

General procedure for the synthesis of compounds **3-28**:

To a solution of 100 mg of compound **2** (0.45 mmol) in 2.5 mL of THF was added 1 equiv. of the appropriate carboxylic acid derivative (0.45 mmol) and 103 mg of *N*-(3-dimethylaminopropyl)-*N'*-ethylcarbodiimide hydrochloride (1 equiv., 0.45 mmol). The solution was stirred at reflux for 12 hours. After cooling to room temperature, the solution was evaporated to dryness. The crude product was dissolved in 20 mL of ethyl acetate and the solution was washed with 1N hydrochloric acid solution (3x20mL) and then by 10% aqueous sodium carbonate solution. The organic layer was dried over Na_2SO_4 , filtered and the solvent is evaporated *in vacuo*. The resulting crude mixture was washed with Et_2O for compounds **4**, **10** and **23**. Compounds **13**, **16-21** and **24** were used without further purification in the subsequent step. Other compounds were purified by chromatography on silica gel.

Tert-butyl (4-(5-*tert*-butyl-2-hydroxybenzoyl))aminobenzylcarbamate (**3**). Elution : DCM/EtOH 98.5/1.5 v/v; White solid (m= 58 mg, 32% yield); mp: 177-178°C; ¹H NMR (CDCl₃, 300 MHz): δ ppm 1.31 (s, 9H), 1.44 (s, 9H), 4.26 (d, 2H, *J* = 5.9 Hz), 4.89 (bs, 1H), 6.93 (d, 1H, *J* = 8.7 Hz), 7.24 (m, 2H), 7.48 (m, 4H), 8.24 (bs, 1H), 11.0 (s, 1H); ¹³C NMR (CDCl₃, 75 MHz): δ ppm 28.6, 31.4, 31.6, 44.4, 79.9, 114.4, 118.4, 121.9, 122.1, 128.2, 132.3, 136.0, 136.1, 142.0, 156.1, 159.3, 168.7; HPLC, RT= 2.10 min; MS (ESI+): *m/z* 399.3 [M+H]⁺; HRMS calcd for C₂₃H₃₁N₂O₄ 399.2278, found 399.2272.

Tert-butyl (4-(2-hydroxybenzoyl))aminobenzylcarbamate (**4**). White solid (m= 113 mg, 73% yield); mp: 107-171°C; ¹H NMR (DMSO *d*₆, 300 MHz): δ ppm 1.40 (s, 9H), 3.30 (bs, 1H), 4.10 (d, 2H, *J* = 6.0 Hz), 6.96 (m, 2H), 7.23 (d, 2H, *J* = 8.4 Hz), 7.33 (bt, 1H, *J* = 6.0 Hz), 7.44 (td, 1H, *J* = 8.5 Hz, 1.6 Hz), 7.62 (d, 2H, *J* = 8.4 Hz), 7.97 (dd, 1H, *J* = 8.5 Hz, 1.6 Hz), 10.35 (s, 1H); ¹³C NMR (DMSO *d*₆, 75 MHz): δ ppm 28.2, 43.0, 77.7, 117.2, 118.9, 120.9, 127.3, 128.9, 133.6, 136.0, 136.6, 155.7, 158.6, 166.5; HPLC, RT= 1.78 min; MS (ESI+): *m/z* 365.0 [M+Na]⁺, 287.1 [M+H-*t*Bu]⁺; HRMS calcd for C₁₉H₂₃N₂O₄ 343.1652, found 343.1655.

Tert-butyl (4-(3-methyl-2-hydroxybenzoyl))aminobenzylcarbamate (**5**). Elution: DCM/EtOH 92/2 v/v. Light yellow solid (m= 125 mg, 78% yield); mp: 166.2-166.9°C; ¹H NMR (CDCl₃, 400 MHz): δ ppm 1.45 (s, 9H), 2.27 (s, 3H), 4.28 (d, 2H, *J* = 5.7 Hz), 4.85 (bs, 1H), 6.79 (t, 1H, *J* = 7.7 Hz), 7.28 (m, 3H), 7.37 (d, 1H, *J* = 7.7 Hz), 7.50 (d, 2H, *J* = 8.4 Hz), 8.00 (bs, 1H), 12.3 (s, 1H); ¹³C NMR (CDCl₃, 100 MHz): δ ppm 16.0, 28.6, 44.4, 79.9, 113.8, 118.4, 121.7, 123.1, 128.3, 128.4, 135.6, 136.1, 136.2, 156.1, 160.5, 169.1; HPLC, RT= 2.01 min; MS (ESI+): *m/z* 379.2 [M+Na]⁺, 301.2 [M+H-*t*Bu]⁺; HRMS calcd for C₂₀H₂₅N₂O₄ 357.1809, found 357.1811.

Tert-butyl (4-(4-methyl-2-hydroxybenzoyl))aminobenzylcarbamate (**6**). Elution: *n*-Hex/AcOEt 2/1 v/v. Light yellow solid (m= 131 mg, 82% yield); mp: 191.8-192.8°C; ¹H NMR (CDCl₃, 400 MHz): δ ppm 1.45 (s, 9H), 2.33 (s, 3H), 4.28 (d, 2H, *J* = 5.5 Hz), 4.84 (bs, 1H), 6.70 (dd, 1H, *J* = 8.1 Hz, 1.1 Hz), 6.82 (d, 1H, *J* = 1.1 Hz), 7.27 (d, 2H, *J* = 8.4 Hz), 7.39 (d, 1H, *J* = 8.1 Hz), 7.50 (d, 2H, *J* = 8.4 Hz), 7.93 (bs, 1H), 11.94 (s, 1H); ¹³C NMR (CDCl₃, 100 MHz): δ ppm 21.9, 28.6, 44.4, 79.9, 112.1, 119.3, 120.3, 121.6, 125.5, 128.4, 136.1, 136.2, 146.1, 156.1, 162.1, 168.6; HPLC, RT= 1.90 min; MS (ESI+): *m/z* 357.2 [M+H]⁺, 379.1 [M+Na]⁺, 301.2 [M+H-*t*Bu]⁺; HRMS calcd for C₂₀H₂₅N₂O₄ 357.1809, found 357.1809.

Tert-butyl (4-(5-methyl-2-hydroxybenzoyl))aminobenzylcarbamate (**7**). Elution: *n*-Hex/AcOEt 2/1 v/v. Light yellow solid (m= 68 mg, 42% yield); mp: 174.5-175.5°C; ¹H NMR (CDCl₃, 400 MHz): δ ppm 1.45 (s, 9H), 2.32 (s, 3H), 4.28 (d, 2H, *J* = 5.4 Hz), 4.84 (bs, 1H), 6.91 (d, 1H, *J* = 8.4 Hz), 7.22-7.29 (m, 4H), 7.52 (d, 2H, *J* = 8.4 Hz), 7.96 (bs, 1H), 11.71 (s, 1H); ¹³C NMR (CDCl₃, 100 MHz): δ ppm 20.8, 28.6, 44.4, 79.9, 114.4, 115.5, 118.8, 121.6, 123.3, 125.7, 128.4, 135.8, 136.1, 156.1, 159.8, 168.6; HPLC, RT= 1.90 min; MS (ESI+): *m/z* 379.2 [M+Na]⁺, 301.2 [M+H-*t*Bu]⁺; HRMS calcd for C₂₀H₂₅N₂O₄ 357.1809, found 357.1810.

Tert-butyl (4-(6-methyl-2-hydroxybenzoyl))aminobenzylcarbamate (**8**). Elution: *n*-Hex/AcOEt 2/1 v/v. Light yellow solid (m= 33 mg, 21% yield); mp: 149.0-150.0°C; ¹H NMR (CDCl₃, 300 MHz): δ ppm 1.46 (s, 9H), 2.60 (s, 3H), 4.28 (d, 2H, *J* = 5.4 Hz), 4.91 (bs, 1H), 6.76 (d, 1H, *J* = 7.5 Hz), 6.84 (d, 1H, *J* = 8.2 Hz), 7.23 (dd, 1H, *J* = 8.2 Hz, 7.5 Hz), 7.27 (d, 2H, *J* = 8.0 Hz), 7.52 (d, 2H, *J* = 8.0 Hz), 7.72 (s, 1H), 9.85 (bs, 1H); ¹³C NMR (CDCl₃, 75 MHz): δ ppm 22.1, 28.5, 44.3, 78.3, 115.7, 119.0, 121.0, 123.1, 128.4, 132.5, 135.5, 136.1, 136.2, 156.1, 159.2, 168.4; HPLC, RT= 1.60 min; MS (ESI+): *m/z* 379.1 [M+Na]⁺, 301.2 [M+H-*t*Bu]⁺; HRMS calcd for C₂₀H₂₅N₂O₄ 357.1809, found 357.1808.

Tert-butyl (4-(5-bromo-2-hydroxybenzoyl))aminobenzylcarbamate (**9**). Elution: *n*-Hex/AcOEt 4/1 v/v. White solid (m= 24 mg, 12% yield); mp: >300°C ¹H NMR (DMSO *d*₆, 400 MHz): δ ppm 1.93 (s, 9H), 4.10 (d, 2H, *J* = 6.0 Hz), 6.95 (d, 1H, *J* = 8.8 Hz), 7.23 (d, 2H, *J* = 8.3 Hz), 7.37 (t, 1H, *J* = 6.8 Hz), 7.57 (dd, 1H, *J* = 8.8 Hz, 2.6 Hz), 7.62 (d, 2H, *J* = 8.3 Hz), 8.08 (d, 1H, *J* = 2.6 Hz), 10.44 (s, 1H), 11.93 (bs, 1H); ¹³C NMR (CDCl₃, 100 MHz): δ ppm 28.2, 43.0, 77.8, 110.0, 119.6, 119.9, 120.8, 127.3, 131.1, 135.8, 136.2, 136.5, 155.8, 157.6, 164.9; HPLC, RT= 2.00 min; MS (ESI+): *m/z* 443.0 [M+Na]⁺, 445.0 [M+2+Na]⁺, 367.0 [M+H-tBu]⁺, 365.0 [M+H+2-tBu]⁺; HRMS calcd for C₁₉H₂₁BrN₂NaO₄ 443.0577, found 443.0575.

Tert-butyl (4-(5-methoxy-2-hydroxybenzoyl))aminobenzylcarbamate (**10**). White solid (m= 75 mg, 45% yield); ¹H NMR (DMSO *d*₆, 300 MHz): δ ppm 1.39 (s, 9H), 3.76 (s, 3H), 4.10 (d, 2H, *J* = 5.9 Hz), 6.92 (d, 1H, *J* = 8.9 Hz), 7.06 (ddd, 1H, *J* = 9.0 Hz, 9.0 Hz, 3.0 Hz), 7.23 (d, 2H, *J* = 8.3 Hz), 7.37 (bt, 1H, *J* = 5.9 Hz), 7.50 (d, 1H, *J* = 3.0 Hz), 7.62 (d, 2H, *J* = 8.3 Hz), 10.90 (s, 1H); ¹³C NMR (DMSO *d*₆, 75 MHz): δ ppm 28.2, 43.0, 55.7, 77.8, 112.5, 117.3, 118.1, 120.6, 121.0, 127.4, 136.1, 136.6, 151.8, 152.3, 155.8, 166.0; ; HPLC, RT= 1.78 min; MS (ESI+): *m/z* 395.1 [M+Na]⁺, 373.1 [M+H]⁺; 317.1 [M+H-tBu]⁺.

Tert-butyl (4-(4-isopropyl-2-hydroxybenzoyl))aminobenzylcarbamate (**11**). Elution: *n*-Hex/AcOEt 3/1 v/v. White solid (m= 53 mg, 31% yield); ¹H NMR (CDCl₃, 400 MHz): δ ppm 1.60 (d, 6H, *J* = 6.7 Hz), 1.83 (s, 9H), 3.24 (hept., 1H, *J* = 6.7 Hz), 4.64 (d, 2H, *J* = 4.0 Hz), 5.25 (bs, 1H), 7.12 (d, 1H, *J* = 7.1 Hz), 7.60 (d, 2H, *J* = 7.6 Hz), 7.86 (m, 3H), 8.47 (bs, 1H), 12.30 (bs, 1H); ¹³C NMR (CDCl₃, 100 MHz): δ ppm 23.7, 28.6, 34.4, 44.4, 79.9, 112.5, 116.5, 117.9, 121.7, 125.8, 128.3, 136.0, 136.2, 156.2, 156.9, 162.1, 168.6; HPLC, RT= 2.09 min; MS (ESI+): *m/z* 407.1 [M+Na]⁺, 385.2 [M+H]⁺.

Tert-butyl (4-(4-trifluoromethyl-2-hydroxybenzoyl))aminobenzylcarbamate (**12**). Elution DCM/EtOH 99/1 v/v; White solid (m= 114 mg, 62% yield); mp: 179.5-180.5°C; ¹H NMR (CD₃OD, 400 MHz): δ ppm 1.46 (s, 9H), 4.22 (s, 2H), 4.76 (bs, 1H), 7.22 (m, 2H), 7.29 (d, 2H, *J* = 8.4 Hz), 7.63 (d, 2H, *J* = 8.4 Hz), 8.11 (d, 1H, *J* = 8.6 Hz); ¹³C NMR (CD₃OD, 100 MHz): δ ppm 28.8, 44.6, 80.2, 115.2 (d, *J* = 3.7 Hz), 116.5 (d, *J* = 3.7 Hz), 122.0, 122.5, 126.3, 128.7, 131.2, 135.8, 137.8, 158.6, 160.4, 165.2, 167.4; HPLC, RT= 1.86 min; MS (ESI+): *m/z* 433.0 [M+Na]⁺, 411.1 [M+H]⁺, 355.0 [M+H-*t*Bu]⁺; HRMS calcd for C₂₀H₂₂F₃N₂O₄ 411.1526, found 411.1537.

Tert-butyl (4-(4-fluoro-2-hydroxybenzoyl))aminobenzylcarbamate (**13**). Elution DCM/EtOH 99/1 v/v; White solid (m= 37 mg, 23% yield); mp: 155-5-156.5°C; ¹H NMR (CD₃OD, 400 MHz): δ ppm 1.45 (s, 9H), 4.21 (s, 2H), 6.64-6.70 (m, 2H), 7.26 (d, 2H, *J* = 8.4 Hz), 7.59 (d, 2H, *J* = 8.4 Hz), 7.98 (dd, 1H, *J* = 9.4 Hz, 8.4 Hz); ¹⁹F NMR (CD₃OD, 400 MHz): δ ppm -107.1; ¹³C NMR (CD₃OD, 100 MHz): δ ppm 28.9, 44.8, 80.3, 105.2 (d, *J* = 24.2 Hz), 107.6 (d, *J* = 24.2 Hz), 114.8, 122.7, 128.8, 132.1 (d, *J* = 11.1 Hz), 132.5, 137.5, 138.0, 163.3 (d, *J* = 13.3 Hz), 167.4 (d, *J* = 251.3 Hz), 168.4; HPLC, RT= 1.88 min; MS (ESI+): *m/z* 383.1 [M+Na]⁺, 361.1 [M+H]⁺, 305.1 [M+H-*t*Bu]⁺; HRMS calcd for C₁₉H₂₂FN₂O₄ 361.1558, found 361.1554.

Tert-butyl (4-(1-hydroxy-2-naphtoyl))aminobenzylcarbamate (**14**). Elution : *n*-Hex/AcOEt 3/1 v/v; White solid (m= 40 mg, 23% yield); mp: 145-146°C; ¹H NMR (DMSO *d*₆, 300 MHz): δ ppm 1.40 (s, 9H), 4.13 (d, 2H, *J* = 5.9 Hz), 7.27 (d, 2H, *J* = 8.1 Hz), 7.40 (bt, 1H, *J* = 5.9 Hz), 7.46 (d, 1H, *J* = 8.9 Hz), 7.58 (dd, 1H, *J* = 8.1 Hz, 7.1 Hz), 7.68 (m, 3H), 7.92 (d, 1H, *J* = 8.1 Hz), 8.10 (d, 1H, *J* = 9.0 Hz), 8.31 (d, 1H, *J* = 8.1 Hz), 10.92 (bs, 1H); ¹³C NMR (DMSO *d*₆, 75 MHz): δ ppm 28.2, 43.0, 77.8, 107.5, 117.7, 121.1, 123.0, 124.7, 125.9, 127.2, 127.5, 129.1, 136.0, 136.1, 136.7, 155.8, 160.0, 169.4; HPLC, RT= 2.13 min; MS (ESI+): *m/z* 415.1 [M+Na]⁺, 337.0 [M+H-*t*Bu]⁺; HRMS calcd for C₂₃H₂₅N₂O₄ 393.1809, found 393.1807.

Tert-butyl (4-(2-hydroxy-1-naphtoyl))aminobenzylcarbamate (**15**). Elution: DCM/EtOH 98.5/1.5 v/v; White solid (m= 90 mg, 51% yield); mp: 188.5-189.5°C; ¹H NMR (CDCl₃, 300 MHz): δ ppm 1.45 (s, 9H), 4.28 (d, 2H, *J* = 5.6 Hz), 4.88 (bs, 1H), 7.16 (d, 1H, *J* = 9.0 Hz), 7.29 (d, 2H, *J* = 8.8 Hz), 7.36 (dd, 1H, *J* = 7.4 Hz, 6.8 Hz), 7.54 (m, 3H), 7.81 (m, 2H), 8.01 (bs, 1H), 8.14 (d, 1H, *J* = 8.6 Hz), 10.92 (bs, 1H) ; ¹³C NMR (CDCl₃, 75 MHz): δ ppm 28.6, 44.4, 79.9, 110.3, 119.5, 121.0, 122.6, 123.8, 128.4, 128.6, 129.0, 129.7, 130.7, 134.4, 136.2, 136.3, 156.0, 159.7, 168.5; HPLC, RT= 1.74 min; MS (ESI+): *m/z* 415.1 [M+Na]⁺, 337.0 [M+H-*t*Bu]⁺; HRMS calcd for C₂₃H₂₅N₂O₄ 393.1809, found 393.1801.

Tert-butyl (4-(3-hydroxy-2-naphtoyl))aminobenzylcarbamate (**16**). White solid (m= 56 mg, 32% yield); mp: 199-200°C; ¹H NMR (DMSO *d*₆, 400 MHz): δ ppm 1.40 (s, 9H), 4.11 (d, 2H, *J* = 6.1 Hz), 7.25 (d, 2H, *J* = 8.4 Hz), 7.32 (s, 1H), 7.35 (m, 2H), 7.50 (ddd, 1H, *J* = 8.4 Hz, *J* = 6.8 Hz, *J* = 1.0 Hz), 7.69 (d, 2H, *J* = 8.4 Hz), 7.75 (d, 1H, *J* = 8.2 Hz), 7.92 (d, 1H, *J* = 8.2 Hz), 8.51 (s, 1H), 10.65 (bs, 1H); ¹³C NMR (DMSO *d*₆, 100 MHz): δ ppm 28.2, 43.0, 77.7, 110.6, 120.5, 121.6, 123.7, 125.7, 126.8, 127.4, 128.1, 128.7, 130.4, 135.8, 135.9, 137.0, 154.0, 155.8, 165.6; HPLC, RT= 1.99 min; MS (ESI+): *m/z* 415.2 [M+Na]⁺, 337.1 [M+H-*t*Bu]⁺; HRMS calcd for C₂₃H₂₅N₂O₄ 393.1809, found 393.1810.

Tert-butyl (4-(2-naphtoyl))aminobenzylcarbamate (**17**). White solid (m= 61 mg, 36% yield); mp: 182.5-183.5°C; ¹H NMR (CDCl₃, 400 MHz): δ ppm 1.45 (s, 9H), 4.28 (d, 2H, *J* = 5.3 Hz), 4.86 (bs, 1H), 7.28 (d, 2H, *J* = 8.4 Hz), 7.56 (m, 2H), 7.63 (d, 2H, *J* = 8.4 Hz), 7.91 (m, 4H), 8.03 (bs, 1H), 8.36 (s, 1H); ¹³C NMR (CDCl₃, 100 MHz): δ ppm 28.6, 44.5, 79.8, 120.7, 123.8, 127.2, 127.8, 128.0, 128.1, 128.5, 129.0, 129.2, 132.3, 132.8, 135.1, 135.4, 137.4, 156.1, 166.0; HPLC, RT= 1.91 min; MS (ESI+): *m/z* 377.1 [M+H]⁺, 399.1 [M+Na]⁺, 321.3 [M+H-*t*Bu]⁺; HRMS calcd for C₂₃H₂₅N₂O₃ 377.1860, found 377.1855.

Tert-butyl (1*H*-2-indolylcarbonyl)aminobenzylcarbamate (**18**). White solid (m= 67 mg, 41% yield); mp: 207-208°C; ¹H NMR (DMSO *d*₆, 400 MHz): δ ppm 1.40 (s, 9H), 4.10 (s, 2H), 7.06 (t, 1H, *J* = 7.5 Hz), 7.22 (m, 3H), 7.36 (bs, 1H), 7.40 (s, 1H), 7.46 (d, 1H, *J* = 8.3 Hz), 7.66 (d, 1H, *J* = 7.5 Hz), 7.72 (d, 2H, *J* = 8.3 Hz), 10.2 (bs, 1H), 11.76 (bs, 1H); ¹³C NMR (DMSO *d*₆, 100 MHz): δ ppm 28.3, 40.0, 77.7, 103.8, 112.4, 119.8, 120.1, 121.7, 123.7, 127.0, 127.3, 131.6, 135.3, 136.9, 137.5, 155.7, 159.7; HPLC, RT= 1.82 min; MS (ESI+): *m/z* 388.2 [M+Na]⁺, 310.2 [M+H-tBu]⁺; HRMS calcd for C₂₁H₂₄N₃O₃ 366.1812, found 366.1812.

Tert-butyl (4-[(4-oxo-1,4-dihydroquinolin-3-yl)carbonyl]aminobenzylcarbamate (**19**). White solid (m= 48 mg, 27% yield); mp: 238-239°C; ¹H NMR (DMSO *d*₆, 400 MHz): δ ppm 1.40 (s, 9H), 4.08 (d, 2H, *J* = 6.0 Hz), 7.17 (d, 2H, *J* = 8.3 Hz), 7.24 (td, 1H, *J* = 8.1 Hz, 1.1 Hz), 7.33 (t, 1H, *J* = 6.1 Hz), 7.50 (td, 1H, *J* = 8.1 Hz, 1.5 Hz), 7.59 (d, 1H, *J* = 8.1 Hz), 7.66 (d, 2H, *J* = 8.3 Hz), 8.24 (dd, 1H, *J* = 8.1 Hz, 1.1 Hz), 8.87 (s, 1H), 13.64 (s, 1H); ¹³C NMR (DMSO *d*₆, 100 MHz): δ ppm 28.3, 43.1, 77.7, 108.6, 118.9, 122.2, 124.7, 126.7, 127.5, 127.6, 129.3, 133.5, 139.0, 149.3, 151.6, 155.8, 166.1, 174.0; HPLC, RT= 1.67 min; MS (ESI+): *m/z* 394.2 [M+H]⁺, 338.2 [M+H-tBu]⁺; HRMS calcd for C₂₂H₂₄N₃O₄ 394.1761, found 394.1756.

Tert-butyl (4-(3-hydroxypyridin-2-yl))aminobenzylcarbamate (**20**). Light yellow solid (m = 30 mg, 19% yield); mp: 90-92°C; ¹H NMR (CDCl₃, 400 MHz): δ ppm 1.45 (s, 9H), 4.29 (d, 2H, *J* = 5.7 Hz), 7.30 (d, 2H, *J* = 8.4 Hz), 7.31-7.37 (m, 2H), 7.65 (d, 2H, *J* = 8.4 Hz), 8.06 (bs, 1H), 8.10 (dd, 1H, *J* = 4.1 Hz, 1.6 Hz), 9.90 (bs, 1H), 11.89 (s, 1H); HPLC, RT= 1.85 min; MS (ESI+): *m/z* 366.1 [M+Na]⁺.

Tert-butyl (4-(6-methoxy-1-hydroxy-2-naphtoyl))aminobenzylcarbamate (**21**). White solid (m= 34 mg, 18% yield); mp: 205.8-206.3°C; ¹H NMR (CDCl₃, 300 MHz): δ ppm 1.48 (s, 9H), 3.94

(s, 3H), 4.30 (d, 2H, $J = 5.4$ Hz), 4.87 (bs, 1H), 7.07 (d, 1H, $J = 2.3$ Hz), 7.16 (dd, 1H, $J = 9.1$ Hz, 2.4 Hz), 7.20 (d, 1H, $J = 8.1$ Hz), 7.30 (d, 2H, $J = 8.3$ Hz), 7.44 (d, 1H, $J = 9.1$ Hz), 7.55 (d, 2H, $J = 8.3$ Hz), 7.98 (bs, 1H), 8.35 (d, 1H, $J = 9.1$ Hz); ^{13}C NMR (CDCl_3 , 75 MHz): δ ppm 28.6, 44.4, 55.5, 79.3, 105.4, 106.2, 117.6, 118.2, 121.0, 121.6, 121.7, 125.9, 128.4, 136.0, 136.2, 138.6, 142.7, 143.1, 160.6, 161.6; HPLC, RT= 2.14 min; MS (ESI+): m/z 445.2 $[\text{M}+\text{Na}]^+$, 367.1 $[\text{M}+\text{H}-\text{tBu}]^+$; HRMS calcd for $\text{C}_{24}\text{H}_{27}\text{N}_2\text{O}_5$ 423.1914, found 423.1911.

Tert-butyl (4-(7-methoxy-1-hydroxy-2-naphtoyl))aminobenzylcarbamate (**22**). White solid ($m = 30$ mg, 16% yield); ^1H NMR (CDCl_3 , 400 MHz) : δ ppm 1.40 (s, 9H), 3.89 (s, 3H), 4.24 (d, 2H, $J = 5.4$ Hz), 4.81 (bs, 1H), 7.17-7.29 (m, 6H), 7.49 (d, 1H, $J = 8.3$ Hz), 7.60 (d, 1H, $J = 8.9$ Hz), 7.65 (d, 1H, $J = 2.4$ Hz), 7.98 (bs, 1H), 13.38 (s, 1H); ^{13}C NMR (CDCl_3 , 400 MHz) : δ ppm 28.6, 29.9, 44.4, 55.7, 79.9, 102.2, 107.4, 118.5, 118.6, 121.7, 122.0, 126.9, 128.5, 129.1, 131.9, 136.2, 156.1, 158.3, 160.3, 169.5; HPLC, RT= 2.12 min ; MS (ESI+) : m/z 423.1 $[\text{M}+\text{H}]^+$, m/z 845.3 $[2\text{M}+\text{H}]^+$, m/z 440.2 $[\text{M}+\text{NH}_4]^+$.

Tert-butyl (4-(7-methyl-1-hydroxy-2-naphtoyl))aminobenzylcarbamate (**23**). Elution: *n*-Hex/AcOEt 4/1 v/v. White solid ($m = 140$ mg, 77% yield); mp: 188.3-188.9°C; ^1H NMR (CDCl_3 , 500 MHz): δ ppm 1.41 (s, 9H), 2.47 (s, 3H), 4.22 (d, 2H, $J = 5.8$ Hz), 4.84 (bt, 1H), 7.20 (m, 3H), 7.34 (d, 1H, $J = 9.0$ Hz), 7.36 (dd, 1H, $J = 8.4$ Hz, 1.4 Hz), 7.46 (d, 1H, $J = 8.1$ Hz), 7.60 (d, 1H, $J = 8.4$ Hz), 8.05 (bs, 1H), 8.15 (s, 1H), 13.45 (s, 1H); ^{13}C NMR (CDCl_3 , 125 MHz): δ ppm 22.0, 28.6, 44.3, 79.9, 107.0, 118.5, 120.0, 121.8, 123.0, 125.9, 127.4, 128.4, 131.6, 134.8, 136.0, 136.1, 136.2, 156.1, 161.0, 169.5; HPLC, RT= 2.23 min; MS (ESI+): m/z 429.1 $[\text{M}+\text{Na}]^+$, 407.2 $[\text{M}+\text{H}]^+$, 351.1 $[\text{M}+\text{H}-\text{tBu}]^+$; HRMS calcd for $\text{C}_{24}\text{H}_{27}\text{N}_2\text{O}_4$ 407.1965, found 407.1962.

Tert-butyl (4-(7-chloro-1-hydroxy-2-naphthoyl))aminobenzylcarbamate (**24**). White solid (m= 101 mg, 53% yield); RMN ^1H (CDCl_3 , 400 MHz): δ ppm 1.58 (s, 9H), 4.32 (d, 2H, $J = 5.7$ Hz), 4.88 (bs, 1H), 7.33 (m, 3H), 7.48 (d, 1H, $J = 8.8$ Hz), 7.55 (dd, 1H, $J = 8.8$ Hz, 2.2 Hz), 7.57 (d, 2H, $J = 8.3$ Hz), 7.72 (d, 1H, $J = 8.7$ Hz), 8.00 (s, 1H), 8.43 (d, 1H, $J = 2.2$ Hz), 13.51 (s, 1H); RMN ^{13}C (CDCl_3 , 400 MHz): δ ppm 28.6, 44.4, 79.9, 107.7, 118.4, 121.1, 121.7, 123.4, 126.6, 128.5, 129.2, 130.2, 132.4, 134.7, 135.9, 136.4, 156.1, 160.6, 169.0; HPLC, RT= 2,12 min; MS (ESI+): m/z 371.1 $[\text{M}+\text{H}-t\text{Bu}]^+$, 373.1 $[\text{M}+\text{H}-t\text{Bu}+2]^+$, 444.1 $[\text{M}+\text{NH}_4]^+$, 446.1 $[\text{M}+\text{NH}_4+2]^+$, 427.1 $[\text{M}+\text{H}]^+$, 429.1 $[\text{M}+\text{H}+2]^+$.

Tert-butyl (4-(6,7-dimethoxy-1-hydroxy-2-naphthoyl))aminobenzylcarbamate (**25**). ELution: nHex/AcOEt 2/1 v/v. White solid (m= 140 mg, 69% yield); ^1H NMR (CDCl_3 , 400 MHz): δ ppm 1.47 (s, 9H), 4.02 (s, 3H), 4.04 (s, 3H), 4.31 (d, 2H, $J = 5.4$ Hz), 4.87 (bs, 1H), 7.07 (s, 1H), 7.18 (d, 1H, $J = 8.7$ Hz), 7.30 (d, 2H, $J = 8.3$ Hz), 7.36 (d, 1H, $J = 8.8$ Hz), 7.56 (d, 2H, $J = 8.3$ Hz), 7.70 (s, 1H), 8.01 (s, 1H), 13.44 (s, 1H); ^{13}C NMR (CDCl_3 , 100 MHz): δ ppm 28.6, 44.4, 56.2, 56.3, 79.8, 102.9, 106.1, 106.5, 117.3, 119.5, 120.7, 121.7, 128.5, 131.1, 133.0, 136.0, 136.3, 149.6, 152.1, 160.2, 169.5; HPLC, RT= 3.81 min; MS (ESI+): m/z 397.2 $[\text{M}+\text{H}-t\text{Bu}]^+$, 453.3 $[\text{M}+\text{H}]^+$, 475.3 $[\text{M}+\text{Na}]^+$.

Synthesis of *tert*-butyl (4-(5-*tert*-butyl-2-hydroxybenzyl)amino)benzyl)carbamate (**29**).

To a solution of 100 mg of compound **2** (0.45 mmol) in 2.5 mL of ethanol were added 80 mg of aldehyde **26** (0.45 mmol, 1 equiv.). The solution was stirred at reflux for 6 hours. After cooling to room temperature, were added 9 mg of sodium borohydride (0.235 mmol, 0.5 equiv.) and the solution was stirred at room temperature for 1h30. Then, 20 mL of water were added and the solution was extracted with ethyl acetate (3x20 mL). The organic layer was

dried over Na₂SO₄, filtered and the solvent is evaporated *in vacuo* to offer compound **30** as a white solid (m= 110 mg, 64% yield); mp 102.0-103.0°C; ¹H NMR (CDCl₃, 300 MHz): δ ppm 1.29 (s, 9H), 1.44 (s, 9H), 4.19 (d, 2H, *J* = 5.6 Hz), 4.35 (s, 2H), 4.81 (bs, 2H), 6.76 (d, 2H, *J* = 8.4 Hz), 6.81 (d, 1H), 7.12 (m, 3H), 7.21 (dd, 1H, *J* = 8.4 Hz, 2.4 Hz), 11.2 (s, 1H); ¹³C NMR (CDCl₃, 75 MHz): δ ppm 28.6, 31.7, 44.4, 48.8, 64.9, 79.6, 115.8, 116.1, 122.4, 124.9, 125.8, 126.1, 128.8, 130.9, 143.0, 146.9, 154.2; HPLC, RT= 3.57 min; MS (ESI+): *m/z* 329.1 [M+H-tBu]⁺, 385.1 [M+H]⁺, 407.1 [M+Na]⁺; HRMS calcd for C₂₃H₃₃N₂O₃ 385.2486, found 385.2499.

Synthesis of *tert*-butyl 4-[(1-hydroxy-2-naphthoyl)amino]piperidine-1-carboxylate (**52**):

To a solution of 91 mg of compound 1-Boc-4-aminopiperidine (0.45 mmol) in 2.5 mL of THF was added 86 mg of 1-hydroxy-2-naphtoic acid (1 equiv., 0.45 mmol) and 103 mg of EDCI (1 equiv., 0.45 mmol). The solution was stirred at reflux for 12 hours. After cooling to room temperature, the solution was evaporated to dryness. The crude product was dissolved in 20 mL of ethyl acetate and the solution was washed with 1N hydrochloric acid solution (3x20mL) and then by 10% aqueous sodium carbonate solution. The organic layer was dried over Na₂SO₄, filtered and the solvent is evaporated *in vacuo*. The resulting crude mixture was purified by chromatography on silica gel, eluted by *n*Hex/AcOEt 3/1 v/v, to offer compound **52** as a white solid (m= 38 mg, 23% yield); ¹H NMR (CDCl₃, 400 MHz): δ ppm 1.23 (m, 1H), 1.42 (m, 1H), 1.46 (s, 9H), 2.04 (m, 2H), 2.90 (t, 2H, *J* = 12.1 Hz), 4.07-4.19 (m, 3H), 6.25 (d, 1H, *J* = 7.7 Hz), 7.23 (d, 1H, *J* = 8.8 Hz), 7.28 (d, 1H, *J* = 8.9 Hz), 7.50 (td, 1H, *J* = 8.2 Hz, 1.3 Hz), 7.56 (td, 1H, *J* = 8.2 Hz, 1.3 Hz), 7.74 (d, 1H, *J* = 7.8 Hz), 8.40 (d, 1H, *J* = 8.2 Hz), 13.75 (s, 1H); ¹³C NMR (CDCl₃, 100 MHz): δ ppm 28.6, 29.8, 32.2, 47.3, 80.0, 106.6, 118.3, 120.9, 124.0, 125.8, 126.0, 127.4, 129.1, 136.4, 154.8, 160.9, 170.2; HPLC, RT= 2.16 min; MS (ESI+): *m/z* 371.2 [M+H]⁺, 315.2 [M+H-tBu]⁺.

General procedure for the synthesis of compounds **28-51** and **53**.

0.2 mmol of compound **3-25**, **27** or **52** in 5 mL of 6N HCl in dioxane was stirred at room temperature for 1 h 30. The dioxane was evaporated and the crude product was washed with diethyl ether to afford deprotected compound as a hydrochloride salt.

N-(4-(aminomethyl)phenyl)-5-*tert*-butyl-2-hydroxybenzamide hydrochloride (**28**). White solid (m= 54 mg, 80% yield); mp: 268-269°C; ¹H NMR (DMSO *d*₆, 300 MHz): δ ppm 1.30 (s, 9H), 3.56 (s, 1H), 3.99 (s, 2H), 6.97 (d, 1H, *J* = 8.2 Hz), 7.50 (m, 3H), 7.72 (d, 2H, *J* = 7.0 Hz), 7.94 (s, 1H), 8.42 (bs, 3H), 10.52 (s, 1H); ¹³C NMR (DMSO *d*₆, 75 MHz): δ ppm 31.2, 41.8, 66.3, 116.7, 116.9, 120.9, 122.8, 125.5, 129.4, 130.6, 138.3, 141.3, 155.7, 166.3; HPLC, RT= 1.45 min; HRMS calcd for C₁₈H₂₃N₂O₂ 299.1754, found 299.1752.

2-(4-(aminomethylphenyl)aminomethyl)-4-*tert*-butylphenol hydrochloride (**29**). White solid (m= 52 mg, 73% yield); mp: 258-260°C (dec.); ¹H NMR (DMSO *d*₆, 300 MHz): δ ppm 1.20 (s, 9H), 3.93 (d, 2H, *J* = 5.2 Hz), 4.31 (bs, 2H), 6.81 (d, 1H, *J* = 8.4 Hz), 7.15 (m, 3H), 7.42 (m, 3H), 8.45 (bs, 3H), 10.43 (s, 1H); ¹³C NMR (DMSO *d*₆, 75 MHz): δ ppm 31.4, 33.7, 41.7, 46.3, 114.7, 119.0, 120.0, 123.2, 125.8, 127.5, 130.0, 130.3, 140.9, 153.3; HPLC, RT= 1.39 min; HRMS calcd for C₁₈H₂₅N₂O 285.1961, found 285.1954.

N-(4-(aminomethyl)phenyl)-2-hydroxybenzamide hydrochloride (**30**). White solid (m= 45 mg, 81% yield); mp: 275-276°C (dec.); ¹H NMR (DMSO *d*₆, 300 MHz): δ ppm 3.99 (d, 2H, *J* = 4.9 Hz), 6.96 (t, 1H, *J* = 7.5 Hz), 7.04 (d, 1H, *J* = 8.4 Hz), 7.43 (dd, 1H, *J* = 8.4 Hz, 7.2 Hz), 7.49 (d, 2H, *J* = 8.4 Hz), 7.75 (d, 2H, *J* = 8.4 Hz), 8.01 (d, 1H, *J* = 7.2 Hz), 8.45 (bs, 3H), 10.51 (s, 1H); ¹³C NMR (DMSO *d*₆, 75 MHz): δ ppm 41.7, 117.2, 117.5, 119.0, 120.8, 129.2, 129.4, 129.5, 133.6, 138.3,

158.2, 166.4; HPLC, RT= 1.05 min; MS (ESI+): m/z 244.1 $[M+H+1]^+$; HRMS calcd for $C_{14}H_{15}N_2O_2$ 243.1128, found 243.1129.

N-(4-(aminomethyl)phenyl)-3-methyl-2-hydroxybenzamide hydrochloride (**31**). Beige solid (m= 54 mg, 92% yield); mp: 275-276°C; 1H NMR (DMSO d_6 , 400 MHz): δ ppm 2.20 (s, 3H), 4.00 (q, 2H, J = 5.6 Hz), 6.88 (t, 1H, J = 7.7 Hz), 7.38 (d, 1H, J = 7.7 Hz), 7.51 (d, 2H, J = 8.4 Hz), 7.75 (d, 2H, J = 8.4 Hz), 8.00 (d, 1H, J = 7.7 Hz), 8.45 (bs, 3H), 10.59 (s, 1H), 12.53 (s, 1H); ^{13}C NMR (DMSO d_6 , 100 MHz): δ ppm 15.5, 41.7, 114.1, 118.0, 121.9, 125.5, 126.1, 129.4, 130.1, 135.1, 137.8, 159.2, 169.2; HPLC, RT= 1.22 min; HRMS calcd for $C_{15}H_{17}N_2O_2$ 257.1285, found 257.1292.

N-(4-(aminomethyl)phenyl)-4-methyl-2-hydroxybenzamide hydrochloride (**32**). Beige solid (m= 53 mg, 90% yield); mp: 282-283°C (dec.); 1H NMR (DMSO d_6 , 400 MHz): δ ppm 2.30 (s, 3H), 3.98 (q, 2H, J = 5.6 Hz), 6.78 (d, 1H, J = 8.2 Hz), 6.84 (s, 1H), 7.48 (d, 2H, J = 8.4 Hz), 7.74 (d, 2H, J = 8.4 Hz), 7.94 (d, 1H, J = 8.2 Hz), 8.43 (bs, 3H), 10.46 (s, 1H); ^{13}C NMR (DMSO d_6 , 100 MHz): δ ppm 21.1, 41.8, 114.2, 117.5, 120.1, 120.9, 129.0, 129.5, 130.3, 138.3, 144.4, 158.8, 166.7; HPLC, RT= 1.11 min; HRMS calcd for $C_{15}H_{17}N_2O_2$ 257.1285, found 257.1293.

2 *N*-(4-(aminomethyl)phenyl)-5-methyl-2-hydroxybenzamide hydrochloride (**33**). White solid (m= 58 mg, 99% yield); mp: 292-293°C (dec.); 1H NMR (DMSO d_6 , 400 MHz): δ ppm 2.28 (s, 3H), 3.98 (q, 2H, J = 5.4 Hz), 6.92 (d, 1H, J = 8.3 Hz), 7.24 (d, 1H, J = 8.3 Hz), 7.48 (d, 2H, J = 8.4 Hz), 7.74 (d, 2H, J = 8.4 Hz), 7.82 (s, 1H), 8.42 (bs, 3H), 10.49 (s, 1H), 11.61 (s, 1H); ^{13}C NMR (DMSO d_6 , 100 MHz): δ ppm 20.0, 41.8, 117.1, 120.7, 127.7, 129.1, 129.5, 130.2, 134.3, 138.4, 156.1, 166.5; HPLC, RT= 1.13 min; HRMS calcd for $C_{15}H_{17}N_2O_2$ 257.1285, found 257.1289.

N-(4-(aminomethyl)phenyl)-6-methyl-2-hydroxybenzamide hydrochloride (**34**). White solid (m= 58 mg, 99% yield); mp: 251-252°C (dec.); ¹H NMR (CD₃OD, 300 MHz): δ ppm 2.32 (s, 3H), 4.10 (s, 2H), 6.72 (d, 1H, *J* = 8.0 Hz), 6.74 (d, 1H, *J* = 8.0 Hz), 7.13 (t, 1H, *J* = 8.0 Hz), 7.44 (d, 2H, *J* = 8.5 Hz), 7.78 (d, 2H, *J* = 8.5 Hz); ¹³C NMR (DMSO *d*₆, 100 MHz): δ ppm 19.2, 44.0, 114.0, 121.7, 122.1, 126.6, 129.9, 130.6, 131.1, 137.5, 141.0, 155.5, 170.1; HPLC, RT= 0.88 min; HRMS calcd for C₁₅H₁₇N₂O₂ 257.1285, found 257.1287.

N-(4-(aminomethyl)phenyl)-5-bromo-2-hydroxybenzamide hydrochloride (**35**). Yellow solid (m= 71 mg, 99% yield); mp: 309-310°C; ¹H NMR (DMSO *d*₆, 400 MHz): δ ppm 4.00 (s, 2H), 7.01 (d, 1H, *J* = 8.8 Hz), 7.47 (d, 2H, *J* = 8.6 Hz), 7.58 (dd, 1H, *J* = 8.8 Hz, 2.4 Hz), 7.73 (d, 2H, *J* = 8.6 Hz), 8.07 (d, 1H, *J* = 2.4 Hz), 8.32 (bs, 3H), 10.50 (s, 1H), 11.90 (bs, 1H); ¹³C NMR (CDCl₃, 100 MHz): δ ppm 41.8, 110.2, 119.5, 120.7, 129.5, 129.7, 131.4, 135.9, 138.2, 157.1, 164.8; HPLC, RT= 1.21 min; HRMS calcd for C₁₄H₁₄N₂O₂Br 321.0233, found 321.0236.

N-(4-(aminomethyl)phenyl)-5-methoxy-2-hydroxybenzamide hydrochloride (**36**). White solid (m= 55 mg, 90% yield); mp: 277.5-278.5°C; ¹H NMR (DMSO *d*₆, 300 MHz): δ ppm 3.76 (s, 3H), 4.00 (s, 2H), 6.95 (d, 1H, *J* = 8.8 Hz), 7.06 (dd, 1H, *J* = 8.8 Hz, 2.2 Hz), 7.47 (d, 2H, *J* = 8.1 Hz), 7.50 (d, 1H, *J* = 2.2 Hz), 7.74 (d, 2H, *J* = 8.1 Hz), 8.22 (bs, 3H), 10.54 (s, 1H); ¹³C NMR (DMSO *d*₆, 75 MHz): δ ppm 41.8, 55.7, 112.7, 117.5, 118.2, 120.6, 120.8, 129.5, 129.6, 138.3, 151.8, 152.0, 165.9; HPLC, RT= 1.10 min; HRMS calcd for C₁₅H₁₇N₂O₃ 273.1234, found 273.1240.

N-(4-(aminomethyl)phenyl)-4-isopropyl-2-hydroxybenzamide hydrochloride (**37**). White solid (m = 63 mg, 56% yield); mp: 282-283°C; ¹H NMR (DMSO *d*₆, 400 MHz): δ ppm 1.20 (d, 6H, *J* = 6.8 Hz), 2.87 (hept, 1H, *J* = 6.8 Hz), 3.99 (d, 2H, *J* = 3.9 Hz), 6.87 (m, 2H), 7.48 (d, 2H, *J* = 8.3 Hz), 7.74 (d, 2H, *J* = 8.3 Hz), 7.95 (d, 1H, *J* = 7.9 Hz), 8.39 (bs, 3H), 10.5 (s, 1H), 11.97 (bs, 1H); ¹³C

NMR (DMSO d_6 , 100 MHz): δ ppm 23.3, 33.3, 41.8, 114.6, 114.7, 117.4, 120.8, 129.0, 129.4, 138.3, 155.0, 158.8, 166.7; HPLC, RT= 1.33 min; HRMS calcd for $C_{17}H_{21}N_2O_2$ 285.1598, found 285.1603.

N-(4-(aminomethyl)phenyl)-4-trifluoromethyl-2-hydroxybenzamide hydrochloride **(38)**.

White solid (m = 67 mg, 96% yield); mp: 270-272°C (dec.); 1H NMR (DMSO d_6 , 400 MHz): δ ppm 3.99 (bs, 2H), 7.28 (d, 1H, J = 7.9 Hz), 7.39 (s, 1H), 7.48 (d, 2H, J = 8.1 Hz), 7.76 (d, 2H, J = 8.1 Hz), 8.03 (d, 1H, J = 7.9 Hz), 8.38 (bs, 3H), 10.54 (s, 1H), 11.97 (bs, 1H); ^{19}F (DMSO d_6 , 400 MHz): -61.77; ^{13}C NMR (DMSO d_6 , 100 MHz): δ ppm 41.8, 113.4, 115.3, 120.3, 122.1, 123.5, 129.5, 130.7, 132.3, 132.6, 138.4, 157.1, 164.5; HPLC, RT= 1.29 min; MS (ESI+): m/z 312.1 [M+H] $^+$, 294.1 [M+H-NH $_3$] $^+$; HRMS calcd for $C_{15}H_{14}F_3N_2O_2$ 311.1002, found 311.1005.

N-(4-(aminomethyl)phenyl)-4-fluoro-2-hydroxybenzamide hydrochloride **(39)**. White solid (m= 45 mg, 76% yield); mp: 280-281°C; 1H NMR (DMSO d_6 , 400 MHz): δ ppm 3.99 (s, 2H), 6.88-6.80 (m, 2H), 7.48 (d, 2H, J = 8.4 Hz), 7.74 (d, 2H, J = 8.4 Hz), 8.08 (dd, 1H, J = 8.7 Hz, J = 8.7 Hz), 8.36 (bs, 3H), 10.47 (s, 1H), 12.36 (bs, 1H); ^{19}F (DMSO d_6 , 400 MHz): -105.70; ^{13}C NMR (DMSO d_6 , 100 MHz): δ ppm 41.8, 103.8 (d, J = 24.2 Hz), 106.5 (d, J = 24.2 Hz), 114.5, 120.9, 129.4, 129.6, 131.5 (d, J = 11 Hz), 138.2, 160.4 (d, J = 13.2 Hz), 164.8 (d, J = 249 Hz), 165.7; HPLC, RT= 1.09 min; HRMS calcd for $C_{14}H_{14}FN_2O_2$ 261.1034, found 261.1034.

N-(4-(aminomethyl)phenyl)-1-hydroxy-2-naphtamide hydrochloride **(40)**. White solid (m= 63 mg, 99% yield); mp: 277-278°C (dec.); 1H NMR (DMSO d_6 , 300 MHz): δ ppm 4.02 (s, 2H), 7.46 (d, 1H, J = 8.9 Hz), 7.53 (d, 2H, J = 8.3 Hz), 7.59 (d, 1H, J = 7.5 Hz), 7.68 (t, 1H, J = 7.5 Hz), 7.80 (d, 2H, J = 8.3 Hz), 7.92 (d, 1H, J = 8.0 Hz), 8.22 (d, 1H, J = 8.9 Hz), 8.31 (d, 1H, J = 8.3 Hz), 8.48 (bs, 3H), 10.43 (s, 1H); ^{13}C NMR (DMSO d_6 , 75 MHz): δ ppm 41.8, 107.5, 117.8, 122.1, 123.1,

123.2, 124.6, 125.9, 127.5, 129.2, 129.4, 130.2, 136.0, 137.8, 160.0, 169.6; HPLC, RT= 1.45 min;
MS (ESI+): m/z 294.1 [M+H+1]⁺; HRMS calcd for C₁₈H₁₇N₂O₂ 293.1290, found 293.1289.

N-(4-(aminomethyl)phenyl)-2-hydroxy-1-naphtamide hydrochloride (**41**). White powder (m= 57 mg, 97% yield); mp: 248-249°C; ¹H NMR (DMSO *d*₆, 300 MHz): δ ppm 3.98 (d, 2H, *J* = 5.3 Hz), 7.32 (m, 2H), 7.45 (m, 3H), 7.67 (d, 1H, *J* = 8.3 Hz), 7.84 (m, 4H), 8.42 (bs, 3H), 10.22 (bs, 1H), 10.43 (s, 1H); ¹³C NMR (DMSO *d*₆, 75 MHz): δ ppm 41.9, 118.4, 119.1, 122.9, 123.2, 126.9, 127.3, 127.9, 128.6, 129.5, 130.1, 131.3, 139.7, 151.7, 165.8; HPLC, RT= 1.11 min; MS (ESI+): m/z 294.1 [M+H+1]⁺; HRMS calcd for C₁₈H₁₇N₂O₂ 293.1285, found 293.1293.

N-(4-(aminomethyl)phenyl)-3-hydroxy-2-naphtamide hydrochloride (**42**). White powder (m= 40 mg, 61% yield); mp: 299-300°C (dec.); ¹H NMR (DMSO *d*₆, 400 MHz): δ ppm 4.00 (s, 2H), 7.37 (m, 2H), 7.51 (m, 3H), 7.76 (d, 1H, *J* = 8.3 Hz), 7.80 (d, 2H, *J* = 8.4 Hz), 7.94 (d, 1H, *J* = 8.3 Hz), 8.35 (bs, 3H), 8.53 (s, 1H), 10.70 (s, 1H), 11.39 (bs, 1H); ¹³C NMR (DMSO *d*₆, 100 MHz): δ ppm 41.8, 110.6, 120.4, 121.8, 123.7, 125.8, 126.9, 128.1, 128.7, 129.4, 129.6, 130.6, 135.8, 138.7, 153.6, 165.6; HPLC, RT= 1.26 min; HRMS calcd for C₁₈H₁₇N₂O₂ 293.1285, found 293.1286.

N-(4-(aminomethyl)phenyl)-2-naphtamide hydrochloride (**43**). White powder (m= 26 mg, 61% yield); mp: 285-286°C (dec.); ¹H NMR (DMSO *d*₆, 500 MHz): δ ppm 4.00 (q, 2H, *J* = 6.0 Hz), 7.50 (d, 2H, *J* = 8.5 Hz), 7.64 (m, 2H), 7.88 (d, 2H, *J* = 8.5 Hz), 8.01 (dd, 1H, *J* = 7.6 Hz, 1.4 Hz), 8.05 (m, 2H), 8.10 (dd, 1H, *J* = 7.3 Hz, 1.3 Hz), 8.47 (bs, 3H), 8.64 (s, 1H), 10.63 (s, 1H); ¹³C NMR (DMSO *d*₆, 125 MHz): δ ppm 41.9, 120.3, 124.5, 126.9, 127.7, 128.0, 128.1, 128.2, 129.0, 129.2, 129.5, 132.0, 132.1, 134.3, 139.4, 165.7; HPLC, RT= 1.21 min; HRMS calcd for C₁₈H₁₇N₂O₂ 277.1335, found 277.1326.

N-[4-(aminomethyl)phenyl]-1*H*-indole-2-carboxamide (**44**). White solid (m= 40 mg, 76% yield); mp: 291-292°C (dec.); ¹H NMR (DMSO *d*₆, 300 MHz): δ ppm 3.98 (q, 2H, *J* = 5.7 Hz), 7.07 (t, 1H, *J* = 7.8 Hz), 7.22 (t, 1H, *J* = 7.8 Hz), 7.47 (m, 4H), 7.67 (d, 1H, *J* = 8.0 Hz), 7.87 (d, 2H, *J* = 8.6 Hz), 8.40 (bs, 3H), 10.47 (s, 1H), 11.88 (s, 1H); ¹³C NMR (DMSO *d*₆, 100 MHz): δ ppm 41.9, 104.4, 112.4, 119.9, 120.0, 121.8, 123.9, 127.0, 128.9, 129.5, 131.4, 136.8, 139.2, 159.7; HPLC, RT= 1.82 min; HRMS calcd for C₁₆H₁₆N₃O 266.1288, found 266.1284.

N-[4-(aminomethyl)phenyl]-4-oxo-1,4-dihydroquinoline-3-carboxamide (**45**). White solid (m= 65 mg, 99% yield); mp: 287-289°C (dec.); ¹H NMR (DMSO *d*₆, 400 MHz): δ ppm 3.96 (q, 2H, *J* = 5.5 Hz), 7.50 (d, 2H, *J* = 8.4 Hz), 7.53 (td, 1H, *J* = 7.9 Hz, 1.3 Hz), 7.76 (d, 2H, *J* = 8.4 Hz), 7.79-7.86 (m, 2H), 8.31 (d, 1H, *J* = 7.9 Hz), 8.53 (bs, 3H), 8.82 (d, 1H, *J* = 6.7 Hz), 12.56 (s, 1H), 13.62 (d, 1H, *J* = 6.4 Hz); ¹³C NMR (DMSO *d*₆, 100 MHz): δ ppm 41.8, 110.3, 119.2, 119.5, 125.3, 125.4, 125.9, 128.9, 129.9, 133.0, 138.9, 139.1, 143.9, 163.0, 176.3; HPLC, RT= 1.04 min; HRMS calcd for C₁₇H₁₆N₃O₂ 294.1237, found 294.1247.

N-(4-(aminomethyl)phenyl)-3-hydroxypyridine-2-carboxamide hydrochloride (**46**). Beige solid (m= 28 mg, 44% yield); mp: 251-252°C; ¹H NMR (DMSO *d*₆, 300 MHz): δ ppm 4.00 (q, 2H, *J* = 5.4 Hz), 4.78 (bs, 3H), 7.50 (m, 3H), 7.61 (dd, 1H, *J* = 8.5 Hz, 4.3 Hz), 7.87 (d, 2H, *J* = 8.6 Hz), 8.27 (dd, 1H, *J* = 4.3 Hz, 1.1 Hz), 8.35 (bs, 2H), 10.99 (s, 1H); ¹³C NMR (DMSO *d*₆, 75 MHz): δ ppm 41.8, 121.3, 126.5, 129.4, 129.6, 130.2, 131.2, 137.3, 139.8, 157.6, 167.3; HPLC, RT= 0.95 min; HRMS calcd for C₁₃H₁₄N₃O₂ 244.1081, found 244.1102.

N-(4-(aminomethyl)phenyl)-6-methoxy-1-hydroxy-2-naphthamide hydrochloride (**47**). Beige solid (m= 65 mg, 91% yield); mp: 256-257°C (dec.); ¹H NMR (DMSO *d*₆, 300 MHz): δ ppm 3.91 (s, 3H), 4.02 (s, 2H), 7.19 (dd, 1H, *J* = 9.2, 2.5 Hz), 7.35 (m, 2H), 7.51 (d, 2H, *J* = 8.6 Hz), 7.77 (d,

2H, $J = 8.6$ Hz), 8.14 (d, 1H, $J = 9.2$ Hz), 8.20 (d, 1H, $J = 9.2$ Hz), 8.36 (bs, 3H), 10.55 (bs, 1H), 14.00 (s, 1H); ^{13}C NMR (DMSO d_6 , 75 MHz): δ ppm 41.8, 55.4, 105.7, 106.4, 117.0, 117.9, 119.4, 122.0, 123.9, 125.0, 129.4, 130.1, 137.9, 138.1, 159.9, 160.3, 169.7; HPLC, RT= 1.36 min; HRMS calcd for $\text{C}_{19}\text{H}_{19}\text{N}_2\text{O}_3$ 323.1390, found 323.1397.

N-(4-(aminomethyl)phenyl)-7-methoxy-1-hydroxy-2-naphtamide hydrochloride (**48**). White solid (m= 55 mg, 77% yield); mp: 250-251°C; ^1H NMR (DMSO d_6 , 400 MHz): δ ppm 3.91 (s, 3H), 4.02 (q, 2H, $J = 5.0$ Hz), 7.32 (dd, 1H, $J = 8.9$ Hz, 2.6 Hz), 7.42 (d, 1H, $J = 8.8$ Hz), 7.51 (d, 2H, $J = 8.6$ Hz), 7.60 (d, 1H, $J = 2.6$ Hz), 7.79 (d, 2H, $J = 8.6$ Hz), 7.85 (d, 1H, $J = 8.9$ Hz), 8.02 (d, 1H, $J = 8.9$ Hz), 8.36 (bs, 3H), 10.59 (s, 1H), 13.86 (s, 1H); ^{13}C NMR (DMSO d_6 , 100 MHz): δ ppm 41.8, 55.2, 101.5, 107.9, 117.7, 120.6, 121.2, 122.1, 125.6, 129.2, 129.4, 130.1, 131.3, 137.8, 157.4, 158.8, 169.7; HPLC, RT= 1.37 min; HRMS calcd for $\text{C}_{19}\text{H}_{19}\text{N}_2\text{O}_3$ 323.1390, found 323.1403.

N-(4-(aminomethyl)phenyl)-7-methyl-1-hydroxy-2-naphtamide hydrochloride (**49**). White solid (m= 53 mg, 77% yield); mp: 276-278°C (dec.); ^1H NMR (DMSO d_6 , 500 MHz): δ ppm 3.34 (s, 3H), 4.01 (s, 2H), 7.40 (d, 1H, $J = 8.7$ Hz), 7.51 (m, 3H), 7.80 (m, 3H), 8.08 (s, 1H), 8.12 (d, 1H, $J = 8.7$ Hz), 8.44 (bs, 3H), 10.62 (s, 1H), 13.94 (s, 1H); ^{13}C NMR (DMSO d_6 , 125 MHz): δ ppm 21.4, 41.8, 107.5, 117.6, 122.0, 122.1, 122.2, 124.7, 127.4, 129.4, 130.2, 131.2, 134.2, 135.4, 137.8, 159.6, 169.7; HPLC, RT= 1.43 min; HRMS calcd for $\text{C}_{19}\text{H}_{19}\text{N}_2\text{O}_2$ 307.1441, found 307.1452.

N-(4-(aminomethyl)phenyl)-7-chloro-1-hydroxy-2-naphtamide hydrochloride (**50**). White solid (m= 55 mg, 76%); mp: 277-278°C; ^1H NMR (DMSO d_6 , 500 MHz): δ ppm 4.02 (q, 2H, $J = 5.6$ Hz), 7.53 (m, 3H), 7.70 (dd, 1H, $J = 8.8$ Hz, 2.2 Hz), 7.79 (d, 2H, $J = 8.6$ Hz), 7.99 (d, 1H, $J = 8.8$ Hz), 8.24 (m, 2H), 8.39 (bs, 3H), 10.73 (s, 1H); ^{13}C NMR (DMSO d_6 , 100 MHz): δ ppm 108.7,

117.8, 121.8, 122.2, 123.8, 125.4, 129.5, 129.6, 129.9, 130.4, 130.8, 134.4, 137.7, 158.8, 169.3;

HPLC, RT= 1.49 min; HRMS calcd for $C_{18}H_{16}N_2O_2Cl$ 327.0895, found 327.0890.

N-(4-(aminomethyl)phenyl)-6,7-dimethoxy-1-hydroxy-2-naphthamide hydrochloride **(51)**.

White solid (m = 62 mg, 80%); mp: 289-291°C (dec.); 1H NMR (DMSO d_6 , 400 MHz): δ ppm 3.90 (s, 3H), 3.92 (s, 3H), 4.01 (q, 2H, J = 6.0 Hz), 7.31 (d, 1H, J = 8.8 Hz), 7.33 (s, 1H), 7.51 (d, 2H, J = 8.6 Hz), 7.55 (s, 1H), 7.79 (d, 2H, J = 8.6 Hz), 8.03 (d, 1H, J = 8.8 Hz), 8.45 (bs, 3H), 10.53 (s, 1H), 13.85 (s, 1H); ^{13}C NMR (DMSO d_6 , 100 MHz): δ ppm 55.4, 55.6, 66.3, 101.8, 106.1, 106.7, 116.6, 119.2, 121.4, 121.9, 129.4, 130.0, 132.5, 137.9, 149.0, 151.6, 158.8, 169.8; HPLC, RT= 2.28 min; HRMS calcd for $C_{20}H_{21}N_2O_4$ 353.1496, found 353.1496.

1-Hydroxy-*N*-piperidin-4-yl-2-naphthamide **(53)**. White solid (m = 43 mg, 70% yield); mp: 279-280°C; 1H NMR (DMSO d_6 , 400 MHz): δ ppm 1.89-2.02 (m, 4H), 3.02 (m, 2H), 3.33 (d, 2H, J = 12.8 Hz), 4.19 (m, 1H), 7.37 (d, 1H, J = 8.8 Hz), 7.55 (td, 1H, J = 8.1 Hz, 1.1 Hz), 7.63 (td, 1H, J = 8.1 Hz, 1.2 Hz), 7.87 (d, 1H, J = 8.1 Hz), 8.03 (d, 1H, J = 8.8 Hz), 8.25 (d, 1H, J = 8.1 Hz), 8.98 (d, 1H, J = 8.1 Hz), 9.08 (bs, 2H), 14.50 (s, 1H); ^{13}C NMR (DMSO d_6 , 100 MHz): δ ppm 27.9, 44.5, 66.3, 106.9, 117.4, 122.9, 123.0, 124.6, 125.7, 127.4, 128.9, 135.8, 159.7, 170.1; HPLC, RT= 1.28 min; HRMS calcd for $C_{16}H_{19}N_2O_2$ 271.1441, found 271.1439.

Enzymes and chemicals

KLK6 was purchased from R&D Systems® as pro-KLK6. Activation of KLK6 is performed in 50 mM Tris, 0.05% (w/v) Brij-35, pH 8.0. The activation reaction is initiated by lysyl-endopeptidase at 2.5 mU.mL⁻¹ (Wako Bioproducts®). The activation reaction is stopped by diluting KLK6 to 0.5 µg.mL⁻¹ in assay buffer (50 mM Tris, 1 M Citrate, 0.05% (w/v) Brij-35, pH 7.4) to obtain an active KLK6 stock. KLK1 was purchased from R & D Systems® as pro-KLK1.

Activation of KLK1 is performed in 50 mM Tris-HCl, 10mM CaCl₂, 150 mM NaCl, 0.05% Brij-35, pH 7.5. The activation reaction is initiated by bacterial thermolysin at 0.4 µg.mL⁻¹ (Sigma-Aldrich®) and stopped by addition of 100 mM EDTA (Sigma-Aldrich®) to obtain an active KLK1 stock at the same concentration of 100 µg.mL⁻¹. Plasmin (Sigma-Aldrich®) and Caspase-2, Caspase-3, Caspase-6 (Enzo Life Sciences®) were purchased in mature and active form. All enzyme stocks were stored at -20 ° C. KLK4, KLK5, KLK7, KLK8, KLK11, KLK13; thrombin, cathepsin L, matriptase, trypsin, trypsin-3 and tPA were purchased from R&D Systems® as pro-enzymes (KLK4, KLK7, KLK8, KLK11, KLK13) or as mature and active forms (KLK5, thrombin, cathepsin L, matriptase, trypsin-3, tPA). Activation of KLK4, KLK7, KLK8, KLK11 and KLK13 are performed in optimized buffers. The activation reactions for KLK4, KLK7 and KLK11 are initiated bacterial thermolysin at 0.4 µg.mL⁻¹ (Sigma-Aldrich®) and stopped by addition of 100 mM EDTA (Sigma-Aldrich®) to obtain active stocks. All enzyme stocks were stored at -20°C. H-PFR-AMC (KLK1), Boc-VPR-AMC (KLK4, KLK5, KLK8, KLK13, KLK14, Thrombin), Boc-QAR-AMC (KLK6, KLK11, Matriptase, Trypsin, Trypsin-3, Plasmin), Ac-VDVAD-AMC (Caspase-2), Ac-DEVD-AMC (Caspase-3), Ac-VEID-AMC (Caspase-6), Z-LR-AMC (Cathepsin L), Z-GGR-AMC (tPA) substrates were purchased from Bachem®. MeO-Suc-RPY-AMC (KLK7) substrate was purchased from AAT Bioquest®.

Kinetics assays

Compounds were screened on KLK6, KLK1 and plasmin using a using a BMG Fluostar microplate reader (black 96-well microplates). The proteases are preincubated for 15 minutes with each compound (10 µM and 50 µM) or with DMSO (<2%, negative control) in a total volume of 100 µl of 50 mM Tris buffer, 1 M citrate, 0.05% Brij-35, pH 7, 37 ° C. The reaction is triggered by adding the Boc-QAR-AMC (KLK6, plasmin) or H-PFR-AMC (KLK1) fluorogenic

substrate (100 μ M) and followed for 30 minutes at 37°C. The release of the AMC fluorescent group is detected using the following wavelengths: λ_{ex} = 360 nm for the excitation and λ_{em} = 460 nm for the measurement of the emission. The percent inhibition is calculated from equation 1 where V_0 is the initial rate of the DMSO control, the initial rate in the presence of the inhibitor V_i .

$$\% \text{ Inhibition} = (1 - (V_i / V_0)) * 100 \text{ (Eq. 1)}$$

The selected compounds are those for which the inhibition is greater than 50% at a concentration of 10 μ M then the IC_{50} is determined. The inhibitory effect of the compound (%) as a function of its concentration generally follows the Eq. 2 which results in a hyperbole or a sigmoid. The equation is entered in the Kaleidagraph® 4.5 software for curve fitting $f([I]) = \% \text{ Inhibition}$, where $[I]$ is the inhibitor concentration. The concentration ranges of inhibitor were adjusted to inhibitory potency as detected in preliminary screening tests, $[I]$ was from 0.1 μ M to 100 μ M.

The inhibitory activity of compounds was expressed as IC_{50} (inhibitor concentrations giving 50% inhibition). The values of IC_{50} were calculated by fitting the experimental data to the Equation 2a and 2b:

$$\% \text{ Inhibition} = 100 \times (1 - V_i / V_0) = 100 [I]_0 / (IC_{50} + [I]_0), \text{ (Eq 2a)}$$

$$\% \text{ Inhibition} = 100 [I]_0^{n_H} / (IC_{50}^{n_H} + [I]_0^{n_H}), \text{ where } n_H \text{ is the Hill number. (Eq 2b)}$$

Reversibility was analysed by diluting the reaction mixtures (dilution factor of 100) after 15 and 60 min preincubation of the enzyme with inhibitor. Aliquots of reaction mixtures (2.5 μ L) were added to 97.5 μ L of buffer containing the fluorogenic substrate (experimental conditions identical to the routine protocol used for a given enzyme). The mechanism of inhibition was determined by varying substrate and inhibitor concentrations, the type of inhibition and inhibition parameter (K_i) are determined by Dixon's plots.

Selectivity profiling

Hit compounds were screened on the selected group of CNS proteases using optimized concentrations and buffers (KLK4 9.6 nM; KLK5 0.85 nM; KLK7 19 nM; KLK8 0.88 nM; KLK11 67 nM; KLK13 0.2 nM; KLK14 0.6 nM; Caspase-2 0.2 nM; Caspase-3 0.1 nM; Caspase-6 68.5 mU. μ L⁻¹; Cathepsin L 0.12 nM; Matriptase 0.69 nM; Thrombin 25 pM; tPA 6.7 nM; Trypsin 0.63 pM ;Trypsin-3 0.8 pM ;Plasmin 3 nM). The reaction is triggered by the appropriate substrate at the optimized concentration (H-PFR-AMC 100 μ M; Boc-VPR-AMC 100 μ M; Boc-QAR-AMC 100 μ M; Meo-Suc-RPY-AMC 100 μ M; Ac-VDVAD-AMC 25 μ M; Ac-DEVD-AMC 10 μ M; Ac-VEID-AMC 100 μ M; Z-LR-AMC 50 μ M; Z-GGR-AMC 100 μ M) and followed for 30 minutes at 37°C. Percentages of inhibition at 10 μ M of each compound are determined as described in previous paragraph. Results are given from 3 independent experiments with a standard error below 10%.

Molecular docking

Molecular docking experiments were conducted to propose interaction models of the hit *para*-aminobenzyl derivatives **32** and **42** with KLK6. The protonation states of the ligands were calculated using MarvinSketch® at pH = 7. The major microspecy described the primary amine function charged, while the rest of the molecules was neutral (protonated alcohol function). The 3D conformations of both ligands were generated by MarvinSketch®. The structure of the target was retrieved from the Protein Data Bank, and chose due to the presence of an orthosteric inhibitor similar in structure to the *para*-aminobenzyl derivatives in order to shape the binding pocket to these two compounds (PDB id: 4D8N^{33, 45}). The protonation state of the target was predicted with Propka.⁴⁶ The catalytic histidine was found charged and protonated

on both nitrogens, while other residues and termini were found in their canonical state at pH 7. The ligands and target were prepared using Autodock Tools 4⁴⁷ before flexible molecular docking with Autodock Vina.⁴⁸ Q192 and S195 side chains were found in different orientations in other KLK6 structures. These two residues were set flexible in the molecular docking routine in order to increase the reliability of the results. Including this protein flexibility, the number of degrees of freedom (dof) was still in an acceptable range for Vina (10 dof, while Vina is designed to converge properly until 12 dof). The box was centered near the geometrical center of the S1 binding pocket (residue: H57, D189 to S195, S214 to N217, C220), with a final size of 18x19x18 Å³ which largely included S1, S1', S2 and S2'. 20 poses were asked with an exhaustiveness of 128. The poses were then re-scored using Convex-PL⁴⁹ and the best poses according to this new scoring function of both compounds into KLK6 were further analyzed. The coordinate files of both poses are available in the online version.

Neuronal cytotoxicity of hit compounds

All animals were ethically maintained and used in compliance with the European Policy on Ethics. Cortices and striatum were microdissected from E14 embryos of Swiss mice (Janvier, Labs Le Genest Saint Isle, France) in D-PBS supplemented with 0.1% (w/w) glucose (ThermoFisher Scientific; 15023-021). Dissected structures were digested with trypsin/EDTA (ThermoFisher Scientific; R001100) for 15 minutes at room temperature. After trypsin inactivation with 10% (v/v) fetal bovine serum (10500056; ThermoFisher Scientific), structures were mechanically dissociated with a pipette in Neurobasal media (ThermoFisher Scientific; 2110349) supplemented with DNase I (ThermoFisher Scientific; EN0525), B27 (ThermoFisher Scientific; 17504-044); L-Glutamine (ThermoFisher Scientific; 25030-024), Penicillin/Streptomycin (ThermoFisher Scientific, 1540-122). Cortical and striatal cells were

then seeded at the density of 100 000 cells/well in sterile transparent 96 well plates previously coated. Cells are cultured for 7 days at 37°C in a 5% CO₂ atmosphere. Cells were treated for 24 hours either with inhibitors at different concentrations (10, 25, 50 or 100 µM) or with the vehicle DMSO 1% (negative control, vehicle) or with rotenone 50 µM (positive control). The treatment of primary cultures of neurons by rotenone is a standard compound used to induce neuronal death. Medium is then replaced with 50 µL of XTT (0.3 mg.mL⁻¹) for 3 hours in order to carry out the cell viability test (Merck; 11465015001). XTT is a derivative of tetrazolium salt whose reduction by mitochondrial dehydrogenase viable cells shows a yellow-orange coloring. The activity of the mitochondria is determined by measuring the absorbance at 485 nm. The percentage of cell survival is calculated by the ratio of the absorbance in the presence of the inhibitor to the negative control condition (DMSO 1%). Statistical analyses of differences between treatments were assessed by a Kruskal-Wallis test using GraphPad Prism 7.03. For all analysis * p-value < 0.05; ** p-value < 0.01; *** p-value < 0.001.

Evaluation of the effect of compounds on oligodendrocyte differentiation

B104 cell culture

B104 cells were cultured in flasks (TPP) containing DMEM (Gibco) supplemented with 1% penicillin-streptomycin (Gibco), 1% Non-Essential Amino Acids Solution (Gibco) and 10% Fetal Bovine Serum (FBS; Gibco) and passaged every week using Trypsin 0.25% (Gibco; 25200056). This medium was changed after 4 days for N1 medium w/o biotin. This B104-conditioned medium containing growth factors was collected after 3 days and used to prepare N1B104 medium.

1
2
3
4
5
6
7
8
9
10
11
12
13
14
15
16
17
18
19
20
21
22
23
24
25
26
27
28
29
30
31
32
33
34
35
36
37
38
39
40
41
42
43
44
45
46
47
48
49
50
51
52
53
54
55
56
57
58
59
60

CG4 cell line culture

CG4 cells were cultured in culture flasks (TPP) coated with 0.01% Poly-L-Ornithine (Sigma) with filtered N1B104 medium to ensure proliferation. Cells were passaged with Trypsin 0.05% (Gibco) when reaching 60-70% confluence.⁵² The CG4 line used in this study expressed the fluorescent reporters GFP at all developmental stages of the oligodendroglial cell lineage and mCherry only in differentiated and mature oligodendrocytes (Deboux *et al.* in preparation). For differentiation assay, CG4 cells were seeded in N1B104 medium in 96 well plates (Nunc) at the density of 6500 cell/cm² for few hours. Cells were then switched in a differentiation medium (DMEM/F12 1:1 (Gibco) supplemented with 2% B27 (Gibco); 1% laminin (Sigma) and 1% N1 biotin) with or without the compounds. The 9-cis-retinoic acid at 1μM (Sigma) was as positive control. Cells were differentiated for 5 days before image acquisition and quantification on an Arrayscan XTI System (Thermo Scientific).

Oligodendrocyte precursor cell (OPCs) primary cell cultures

Primary OPCs cultured were derived from Wistar rats' cerebral cortices at P1, as previously described.⁵⁰ Briefly, the cerebral cortices were dissected and the meninges were removed in DME, 1% penicillin-streptomycin and 1% MEM NEAA. Tissues were dissociated enzymatically using trypsin-EDTA solution for 10 min at 37°C. Cell suspension was filtered with 70 μm nylon cell strainer, centrifuged at 1000 rpm for 10 min and resuspended in an appropriate volume of DMEM/10% FBS for seeding (10 ml per flask/ 2 brains in each) in culture flasks coated with 0.01% poly-L-ornithine and incubated at 5% CO₂ and 37°C for approximately two weeks. The medium was changed at day 7. After 14 DIV, cells were shaken for 2h at 250 rpm to remove microglia⁵¹. An additional shaking is performed overnight at 250 rpm to detach and collect OPCs. Collected OPCs were plated on Poly-Ornithine coated 24-well plates, at a density of 25

000 cells/well. OPCs were kept in proliferation medium containing DMEM/F12 (1:1), supplemented with 2% B27 (all purchased from Gibco), FGF and PDGF (10 ng/ml each) to allow adhesion. The medium is then changed for a differentiation medium with or without the compounds. As for the CG4 cultures, 9-cis-retinoic acid at 1 μ M was used as a positive control. Cells were kept in differentiation medium for 5 days, before image acquisition and quantification on an Arrayscan XTI System (Thermo Scientific).

Immunostaining

Cells were fixed with 2% paraformaldehyde (Electron Microscopy) for 5mn at room temperature, washed with PBS 1X and stored at 4°C prior to staining. They were incubated for 1 hour at RT in 4% BSA (Sigma); 1X PBS, 0.1% Triton X-100 and primary antibodies. They were next rinsed three times with PBS 1X and incubated for 45mn at RT in 4% BSA in 1X PBS, 1 μ g/ml Hoechst dye (Sigma, B2261) and secondary antibodies. After incubation, plates were washed three times with PBS 1X. Image acquisitions and quantification were performed as described above.

The line used is a rat oligodendrocyte precursor (CG4) CG4 cell line, stably transduced with the GFP reporter gene under the control of the CMV promoter and mCherry under the control of a differentiated oligodendrocyte specific promoter. The mCherry marker is only expressed at the differentiated oligodendrocyte stage and thus makes it possible to test compounds capable of inducing differentiation of OPCs. The cells are cultured in the proliferation medium described by Louis et al.⁵² at the time of their enumeration, then in a medium of differentiation (DMEM / F12, B27, N1, biotin, laminin). The cells are treated with different inhibitor concentrations for 72 h in 96-well plates and then screened using an automated inverted microscope. The experimental controls used are a basal control containing only the

1
2
3
4
5
6
7
8
9
10
11
12
13
14
15
16
17
18
19
20
21
22
23
24
25
26
27
28
29
30
31
32
33
34
35
36
37
38
39
40
41
42
43
44
45
46
47
48
49
50
51
52
53
54
55
56
57
58
59
60

differentiation medium and a positive control, 9-cis-retinoic acid, known for its effect in inducing differentiation of OPCs.⁵³ To evaluate the effects of the compounds on OPC differentiation, we quantified the number of mCherry+ and GFP+ cells in each experimental condition relatively to the basal control. An effect in favor of differentiation is reflected in a significant increase in the number of mCherry+ cells, in contrast to an effect to the detriment of differentiation. The results are analyzed using the Mann-Whitney statistical test.

Anti-inflammatory potential

The impact of compounds on microglial activation and pro-inflammatory cytokines was assessed in purified primary microglial cultures isolated from newborn rat brain, as previously described.³⁶ All animals used were handled in accordance with European standards for ethics and animal welfare. The new born WISTAR rats (Janvier Labs®, Le Genest Saint Isle, France) at stage P1 are sacrificed by decapitation. After removal of the meninges, the cortical structures are removed in DMEM medium containing 1% of penicillin / streptomycin mix (Thermofisher®, 15070063) and 1% of non-essential amino acids (MEM NEAA, Thermofisher®, 11140050). Tissues are enzymatically dissociated by the addition of trypsin-EDTA (Gibco®, 25200056) for 10 minutes at 37 ° C. Cell suspension is then passed through a nylon filter 70 µm in diameter, centrifuged at 1000 rpm for 10 minutes then resuspended in a volume of 10 mL of DMEM medium supplemented with 10% FCS (Thermofisher Scientific®, 10500056) in a flask previously coated with 0.01% poly-L-ornithine (Sigma-Aldrich®, P4957). Cells are cultured for two weeks at 37 ° C in a humid atmosphere (5% CO₂) with a change of medium on the seventh day. At the end of this period, the cells are stirred for 2 hours at 250 rpm to detach and recover the microglia. Cells are inoculated into sterile transparent 96-well FALCON® plates at a density of 50,000 cells / well in DMEM / F12 medium supplemented with 1% N2 mix, then cultured for 24 hours at 37 ° C in a humid atmosphere (5% CO₂). The microglia is treated with lipopolysaccharide (LPS, 10 ng.mL⁻¹, Sigma Aldrich®) to create an inflammatory environment to be

1
2
3 activated. Concomitantly, cells are treated either with inhibitors at different concentrations defined
4
5 according to the IC_{50} values (0.5 – 10 μ M), or with 1% DMSO (negative control), or with 100 nM
6
7 dexamethasone (positive anti-inflammatory control, Sigma -Aldrich® D4902) for 3 hours at 37 ° C in a
8
9 humid atmosphere (5% CO_2). At the end of this incubation, supernatants are recovered for assays of
10
11 pro-inflammatory cytokines TNF- α and IL1- β by ELISA (Rat TNF- α ELISA MAX™ Deluxe Set # 438204,
12
13 rat IL1- β ELISA kit ab100768)
14
15
16
17
18
19
20
21
22
23
24
25
26
27
28
29
30
31
32
33
34
35
36
37
38
39
40
41
42
43
44
45
46
47
48
49
50
51
52
53
54
55
56
57
58
59
60

Associated content

The supporting information is available free of charge on the ACS Publications website.

Supplementary figures: compounds synthesis and characterization data, Dixon plot of compounds **37** and **47** towards KLK6 (**Figure S1**), Structure of synthesized compounds (**Table S1**), comparative table of ADME and pharmacological parameters for hit compounds **32** and **42** (**Table S2**).

Models of compounds **32** and **42** docked on 4D8N KLK6 pdb files. (PDB)

Molecular formula strings of compounds described in this study (CSV)

Author information

Corresponding authors

Email: Chahrazade.el_amri@sorbonne-universite.fr

Address

Sorbonne Université, Faculty of Sciences and Engineering, IBPS, UMR 8256 CNRS-UPMC, ERL INSERM U1164, Biological Adaptation and Ageing, F-75252 Paris, France. Paris, France

Author contributions

The research was designed by CE, NM, BNO. Chemical synthesis was performed by NM. Enzymology assays were performed by SAA, NC and FS, biological with neural cells, OPCs and microglial by SAA and CD. Docking models were determined by ML. ED and SB contributed to experiments on primary cultures of neural cells. Data analysis and manuscript preparation were done by CE, NM and BNO. All the authors have given approval the final version of the manuscript.

Notes

The authors declare no competing financial interest.

Acknowledgements:

The authors are grateful to Sorbonne Université, Université of Montpellier, Institut National pour la Recherche Médicale (INSERM), Centre National de la Recherche Scientifique (CNRS) as well as the SATT Lutech for research funding. The authors wish to thank Dr David Akbar (ICM Cell Culture Facility, CELIS) for his advice and technical assistance on fluorescence imaging and quantitative analysis. This study was supported by the Investissements d'Avenir ANR-10-IAIHU-06 (IHU-A-ICM) and ANR-11-INBS-0011 (NeurATRIS) (to B.N-O.) We also thank the French Ministry of Research and Education for S A and F. S PhD fellowships.

Abbreviations used

ADMET, Absorption Diffusion Metabolism, Elimination and Toxicity; CNS, central nervous system; DMEM, Dulbecco's modified Eagle's medium; DMSO, dimethyl sulfoxide; EDCI, N-(3-dimethylaminopropyl)-N'-ethylcarbodiimide hydrochloride; IL1 β : interleukin 1 β ; KLK, tissue kallikreins; KLK1, kallikrein-related peptidase 1; KLK6, kallikrein-related peptidase 6; LPS, lipopolysaccharide; MBP, myelin basic protein; MS, multiple sclerosis; OPC, oligodendrocyte precursor cell; PAR, Protease-Activated receptors; TNF β : tumor necrosis factor.

References

1. Lassmann, H. Multiple Sclerosis Pathology. *Cold Spring Harb Perspect Med* **2018**, 8, 1-15.

2. Frieze, M. A.; Schattling, B.; Fugger, L. Mechanisms of neurodegeneration and axonal dysfunction in multiple sclerosis. *Nat Rev Neurol* **2014**, 10, 225-238.

3. Kuhlmann, T.; Miron, V.; Cui, Q.; Wegner, C.; Antel, J.; Bruck, W. Differentiation block of oligodendroglial progenitor cells as a cause for remyelination failure in chronic multiple sclerosis. *Brain* **2008**, 131, 1749-1758.

4. Bove, R. M.; Green, A. J. Remyelinating Pharmacotherapies in Multiple Sclerosis. *Neurotherapeutics* **2017**, 14, 894-904.

5. Cole, K. L. H.; Early, J. J.; Lyons, D. A. Drug discovery for remyelination and treatment of MS. *Glia* **2017**, 65, 1565-1589.

6. Franklin, R. J. M.; Ffrench-Constant, C. Regenerating CNS myelin - from mechanisms to experimental medicines. *Nat Rev Neurosci* **2017**, 18, 753-769.

7. Coetzee, T.; Thompson, A. J. Unified understanding of MS course is required for drug development. *Nat Rev Neurol* **2018**, 14, 191-192.

8. Cunniffe, N.; Coles, A. Promoting remyelination in multiple sclerosis. *J Neurol* **2021**, 268, 30-44.

9. Murakami, K.; Jiang, Y. P.; Tanaka, T.; Bando, Y.; Mitrovic, B.; Yoshida, S. In vivo analysis of kallikrein-related peptidase 6 (KLK6) function in oligodendrocyte development and the expression of myelin proteins. *Neuroscience* **2013**, 236, 1-11.

10. Bando, Y.; Ito, S.; Nagai, Y.; Terayama, R.; Kishibe, M.; Jiang, Y. P.; Mitrovic, B.; Takahashi, T.; Yoshida, S. Implications of protease M/neurosin in myelination during experimental demyelination and remyelination. *Neurosci Lett* **2006**, 405, 175-180.

11. Scarisbrick, I. A.; Isackson, P. J.; Ciric, B.; Windebank, A. J.; Rodriguez, M. MSP, a trypsin-like serine protease, is abundantly expressed in the human nervous system. *J Comp Neurol* **2001**, 431, 347-361.
12. Bando, Y.; Hagiwara, Y.; Suzuki, Y.; Yoshida, K.; Aburakawa, Y.; Kimura, T.; Murakami, C.; Ono, M.; Tanaka, T.; Jiang, Y. P.; Mitrovi, B.; Bochimoto, H.; Yahara, O.; Yoshida, S. Kallikrein 6 secreted by oligodendrocytes regulates the progression of experimental autoimmune encephalomyelitis. *Glia* **2018**, 66, 359-378.
13. Burda, J. E.; Radulovic, M.; Yoon, H.; Scarisbrick, I. A. Critical role for PAR1 in kallikrein 6-mediated oligodendrogliopathy. *Glia* **2013**, 61, 1456-1470.
14. Yoon, H.; Radulovic, M.; Scarisbrick, I. A. Kallikrein-related peptidase 6 orchestrates astrocyte form and function through proteinase activated receptor-dependent mechanisms. *Biol Chem* **2018**, 399, 1041-1052.
15. Yoon, H.; Radulovic, M.; Walters, G.; Paulsen, A. R.; Drucker, K.; Starski, P.; Wu, J.; Fairlie, D. P.; Scarisbrick, I. A. Protease activated receptor 2 controls myelin development, resiliency and repair. *Glia* **2017**, 65, 2070-2086.
16. Radulovic, M.; Yoon, H.; Wu, J.; Mustafa, K.; Scarisbrick, I. A. Targeting the thrombin receptor modulates inflammation and astrogliosis to improve recovery after spinal cord injury. *Neurobiol Dis* **2016**, 93, 226-242.
17. Panos, M.; Christophi, G. P.; Rodriguez, M.; Scarisbrick, I. A. Differential expression of multiple kallikreins in a viral model of multiple sclerosis points to unique roles in the innate and adaptive immune response. *Biol Chem* **2014**, 395, 1063-1073.
18. Kroksveen, A. C.; Aasebo, E.; Vethe, H.; Van Pesch, V.; Franciotta, D.; Teunissen, C. E.; Ulvik, R. J.; Vedeler, C.; Myhr, K. M.; Barsnes, H.; Berven, F. S. Discovery and initial verification

of differentially abundant proteins between multiple sclerosis patients and controls using iTRAQ and SID-SRM. *J Proteomics* **2013**, 78, 312-325.

19. Scarisbrick, I. A. The multiple sclerosis degradome: enzymatic cascades in development and progression of central nervous system inflammatory disease. *Curr Top Microbiol Immunol* **2008**, 318, 133-175.

20. Blaber, S. I.; Ciric, B.; Christophi, G. P.; Bennett, M. J.; Blaber, M.; Rodriguez, M.; Scarisbrick, I. A. Targeting kallikrein 6 proteolysis attenuates CNS inflammatory disease. *FASEB J* **2004**, 18, 920-932.

21. Yoon, H.; Blaber, S. I.; Evans, D. M.; Trim, J.; Juliano, M. A.; Scarisbrick, I. A.; Blaber, M. Activation profiles of human kallikrein-related peptidases by proteases of the thrombostasis axis. *Protein Sci* **2008**, 17, 1998-2007.

22. Shaw, M. A.; Gao, Z.; McElhinney, K. E.; Thornton, S.; Flick, M. J.; Lane, A.; Degen, J. L.; Ryu, J. K.; Akassoglou, K.; Mullins, E. S. Plasminogen Deficiency Delays the Onset and Protects from Demyelination and Paralysis in Autoimmune Neuroinflammatory Disease. *J Neurosci* **2017**, 37, 3776-3788.

23. Balashov, K.; Dhib-Jalbut, S.; Rybinnik, I. Fibrinolysis induced clinical improvement in a patient with multiple sclerosis exacerbation. *Mult Scler Relat Disord* **2020**, 43, 102225.

24. Masurier, N.; Arama, D. P.; El Amri, C.; Lisowski, V. Inhibitors of kallikrein-related peptidases: An overview. *Med Res Rev* **2018**, 38, 655-683.

25. Prassas, I.; Eissa, A.; Poda, G.; Diamandis, E. P. Unleashing the therapeutic potential of human kallikrein-related serine proteases. *Nat Rev Drug Discov* **2015**, 14, 183-202.

26. Masurier, N.; Soualmia, F.; Sanchez, P.; Lefort, V.; Roué, M.; Maillard, L.; Subra, G.; Percot, A.; El Amri, C. Synthesis of Peptide–Adenine Conjugates as a New Tool for Monitoring Protease Activity. *Eur. J. Org. Chem* **2019**, 2019, 176-183.

- 1
2
3 27. Loessner, D.; Goettig, P.; Preis, S.; Felber, J.; Bronger, H.; Clements, J. A.; Dorn, J.;
4
5 Magdolen, V. Kallikrein-related peptidases represent attractive therapeutic targets for ovarian
6
7 cancer. *Expert Opin Ther Targets* **2018**, 22, 745-763.
8
9
10 28. Goettig, P.; Magdolen, V.; Brandstetter, H. Natural and synthetic inhibitors of
11
12 kallikrein-related peptidases (KLKs). *Biochimie* **2010**, 92, 1546-1567.
13
14
15 29. Sananes, A.; Cohen, I.; Shahar, A.; Hockla, A.; De Vita, E.; Miller, A. K.; Radisky, E. S.;
16
17 Papo, N. A potent, proteolysis-resistant inhibitor of kallikrein-related peptidase 6 (KLK6) for
18
19 cancer therapy, developed by combinatorial engineering. *J Biol Chem* **2018**, 293, 12663-
20
21 12680.
22
23
24 30. De Vita, E.; Schuler, P.; Lovell, S.; Lohbeck, J.; Kullmann, S.; Rabinovich, E.; Sananes, A.;
25
26 Hessling, B.; Hamon, V.; Papo, N.; Hess, J.; Tate, E. W.; Gunkel, N.; Miller, A. K. Depsipeptides
27
28 Featuring a Neutral P1 Are Potent Inhibitors of Kallikrein-Related Peptidase 6 with On-Target
29
30 Cellular Activity. *J Med Chem* **2018**, 61, 8859-8874.
31
32
33 31. Soualmia, F.; Bosc, E.; Aït Amiri, S.; Stratmann, D.; Magdolen, V.; Darmoul, D.; Reboud-
34
35 Ravaux, M.; El Amri, C. Insights into the activity control of the kallikrein-related peptidase 6:
36
37 small-molecule modulators and allostereism. *Biol Chem.* **2018**, 399, 1073-1078.
38
39
40 32. De Vita, E.; Smits, N.; van den Hurk, H.; Beck, E. M.; Hewitt, J.; Baillie, G.; Russell, E.;
41
42 Pannifer, A.; Hamon, V.; Morrison, A.; McElroy, S. P.; Jones, P.; Ignatenko, N. A.; Gunkel, N.;
43
44 Miller, A. K. Synthesis and Structure-Activity Relationships of N-(4-Benzamidino)-
45
46 Oxazolidinones: Potent and Selective Inhibitors of Kallikrein-Related Peptidase 6.
47
48 *ChemMedChem* **2020**, 15, 79-95.
49
50
51 33. Liang, G.; Chen, X.; Aldous, S.; Pu, S. F.; Mehdi, S.; Powers, E.; Xia, T.; Wang, R. Human
52
53 kallikrein 6 inhibitors with a para-amidobenzylamine P1 group identified through virtual
54
55 screening. *Bioorg Med Chem Lett* **2012**, 22, 2450-2455.
56
57
58
59
60

- 1
2
3 34. Skaper, S. D. Oligodendrocyte precursor cells as a therapeutic target for demyelinating
4 diseases. *Prog Brain Res* **2019**, 245, 119-144.
5
6
7
8 35. Voet, S.; Prinz, M.; van Loo, G. Microglia in Central Nervous System Inflammation and
9 Multiple Sclerosis Pathology. *Trends Mol Med* **2019**, 25, 112-123.
10
11
12 36. Tamashiro, T. T.; Dalgard, C. L.; Byrnes, K. R. Primary microglia isolation from mixed
13 glial cell cultures of neonatal rat brain tissue. *J Vis Exp* **2012**, 15, e3814.
14
15
16 37. Bowes, J.; Brown, A. J.; Hamon, J.; Jarolimek, W.; Sridhar, A.; Waldron, G.; Whitebread,
17 S. Reducing safety-related drug attrition: the use of in vitro pharmacological profiling. *Nat Rev*
18 *Drug Discov* **2012**, 11, 909-922.
19
20
21 38. Strauss, K. I. Antiinflammatory and neuroprotective actions of COX2 inhibitors in the
22 injured brain. *Brain Behav Immun* **2008**, 22, 285-98.
23
24
25 39. Katayama, K.; Arai, Y.; Murata, K.; Saito, S.; Nagata, T.; Takashima, K.; Yoshida, A.;
26 Masumura, M.; Koda, S.; Okada, H.; Muto, T. Discovery and structure-activity relationships of
27 spiroindolines as novel inducers of oligodendrocyte progenitor cell differentiation. *Bioorg*
28 *Med Chem* **2020**, 28, 115348.
29
30
31 40. Zaldivar-Diez, J.; Li, L.; Garcia, A. M.; Zhao, W. N.; Medina-Menendez, C.; Haggarty, S.
32 J.; Gil, C.; Morales, A. V.; Martinez, A. Benzothiazole-Based LRRK2 Inhibitors as Wnt Enhancers
33 and Promoters of Oligodendrocytic Fate. *J Med Chem* **2020**, 63, 2638-2655.
34
35
36 41. Su, W.; Matsumoto, S.; Banine, F.; Srivastava, T.; Dean, J.; Foster, S.; Pham, P.;
37 Hammond, B.; Peters, A.; Girish, K. S.; Rangappa, K. S.; Basappa, J. J.; Hennebold, J. D.; Murphy,
38 M. J.; Bennett-Toomey, J.; Back, S. A.; Sherman, L. S. A modified flavonoid accelerates
39 oligodendrocyte maturation and functional remyelination. *Glia* **2020**, 68, 263-279.
40
41
42 42. Darensbourg, D. J.; Chung, W. C.; Arp, C. J.; Tsai, F. T.; Kyran, S. J. Copolymerization and
43 Cycloaddition Products Derived from Coupling Reactions of 1,2-Epoxy-4-cyclohexene and
44
45
46
47
48
49
50
51
52
53
54
55
56
57
58
59
60

Carbon Dioxide. Postpolymerization Functionalization via Thiol–Ene Click Reactions. *Macromolecules* **2014**, 47, 7347–7353.

43. Tanaka, K. I.; Yoshifuji, S.; Nitta, Y. A New Method for the Synthesis of Amides from Amines : Ruthenium Tetroxide Oxidation of N-Protected Alkylamines. *Chemical & pharmaceutical bulletin* **1988**, 36, 3125-3129.

44. Gallo-Rodriguez, C.; Ji, X. D.; Melman, N.; Siegman, B. D.; Sanders, L. H.; Orlina, J.; Fischer, B.; Pu, Q.; Olah, M. E.; van Galen, P. J.; Stiles, G. L.; Jacobson, K. A. Structure-activity relationships of N6-benzyladenosine-5'-uronamides as A3-selective adenosine agonists. *J Med Chem* **1994**, 37, 636-646.

45. Liang, G.; Chen, X.; Aldous, S.; Pu, S. F.; Mehdi, S.; Powers, E.; Giovanni, A.; Kongsamut, S.; Xia, T.; Zhang, Y.; Wang, R.; Gao, Z.; Merriman, G.; McLean, L. R.; Morize, I. Virtual Screening and X-ray Crystallography for Human Kallikrein 6 Inhibitors with an Amidinothiophene P1 Group. *ACS Med Chem Lett* **2012**, 3, 159-164.

46. Olsson, M.; Søndergaard, C. R.; Rostkowski, M.; Jensen, J. H. PROPKA3: Consistent Treatment of Internal and Surface Residues in Empirical pKa Predictions. *Journal of Chemical Theory and Computation* **2011**, 7, 525-537.

47. Morris, G. M.; Huey, R.; Lindstrom, W.; Sanner, M. F.; Belew, R. K.; Goodsell, D. S.; Olson, A. J. AutoDock4 and AutoDockTools4: Automated docking with selective receptor flexibility. *J Comput Chem* **2009**, 30, 2785-2791.

48. Trott, O.; Olson, A. J. AutoDock Vina: improving the speed and accuracy of docking with a new scoring function, efficient optimization and multithreading. *J Comput Chem* **2010**, 31, 455-461.

1
2
3
4
5
6
7
8
9
10
11
12
13
14
15
16
17
18
19
20
21
22
23
24
25
26
27
28
29
30
31
32
33
34
35
36
37
38
39
40
41
42
43
44
45
46
47
48
49
50
51
52
53
54
55
56
57
58
59
60

49. Kadukova, M.; Grudinin, S. Convex-PL: a novel knowledge-based potential for protein-ligand interactions deduced from structural databases using convex optimization. *J Comput Aided Mol Des* **2017**, 31, 943-958.

50. Wegener, A.; Deboux, C.; Bachelin, C.; Frah, M.; Kerninon, C.; Seilhean, D.; Weider, M.; Wegner, M.; Nait-Oumesmar, B. Gain of Olig2 function in oligodendrocyte progenitors promotes remyelination *Brain* **2015**, 138, 120-135.

51. de Vellis, J.; Cole, R. Preparation of mixed glial cultures from postnatal rat brain. *Methods Mol Biol* **2012**, 814, 49-59

52. Louis, J. C.; Magal, E.; Muir, D.; Manthorpe, M.; Varon, S. CG-4, a new bipotential glial cell line from rat brain, is capable of differentiating in vitro into either mature oligodendrocytes or type-2 astrocytes. *J Neurosci Res* **1992**, 31, 193-204.

53. Huang, J. K.; Jarjour, A. A.; Nait Oumesmar, B.; Kerninon, C.; Williams, A.; Krezel, W.; Kagechika, H.; Bauer, J.; Zhao, C.; Baron-Van Evercooren, A.; Chambon, P.; Ffrench-Constant, C.; Franklin, R. J. M. Retinoid X receptor gamma signaling accelerates CNS remyelination. *Nat Neurosci* **2011**, 14, 45-53.

Table of content graphic

